Carbohydrate Research 562 (2026) 109833

Contents lists available at ScienceDirect

Carbohydrate Research

journal homepage: www.elsevier.com/locate/carres

Oligosaccharides from *Scorzonera yildirimlii* and *S. zorkunensis*, and their potential antimicrobial, enzyme inhibition, cytotoxic effect, and *in silico* study

Nurettin Yaylı [a,*], Büşra Korkmaz [a], Gozde Bozdal [b,**], Büşra Şahin [c], Şeyma Arıcı [a], Yasemin Altun Ali [d], Sermet Yıldırmış [e], Gökçe Seyhan [e], Ahmet Buğra Aksel [f], Kamil Coşkunçelebi [g], Serdar Makbul [h], Arif Bozdeveci [h]

[a] Department of Pharmacognosy, Faculty of Pharmacy, Karadeniz Technical University, 61080, Trabzon, Türkiye
[b] Department of Pharmaceutical Botany, Faculty of Pharmacy, Karadeniz Technical University, Trabzon, Türkiye
[c] Medicinal-Aromatic Plants Application and Research Centre, Artvin Coruh University, 08000, Artvin, Türkiye
[d] Department of Pharmaceutical Toxicology, Faculty of Pharmacy, Karadeniz Technical University, 61080, Trabzon, Türkiye
[e] Department of Biochemistry, Faculty of Pharmacy, Karadeniz Technical University, 61080, Trabzon, Türkiye
[f] Department of Pharmaceutical Chemistry, Faculty of Pharmacy, Karadeniz Technical University, 61080, Trabzon, Türkiye
[g] Department of Biology, Faculty of Sciences, Karadeniz Technical University, 61080, Trabzon, Türkiye
[h] Department of Biology, Faculty of Sciences and Arts, Recep Tayyip Erdogan University, 53100, Rize, Türkiye

ARTICLE INFO

Keywords:
Scorzonera yildirimlii
Scorzonera zorkunensis
Oligosaccharides
Antimicrobial
Enzyme inhibition
Cytotoxicity
In silico

ABSTRACT

In this study, the phytochemical investigation of *Scorzonera yildirimlii* and *S. zorkunensis* led to the isolation and identification of eight new oligosaccharide constituents (**1**–**8**). Their structures were elucidated through comprehensive spectroscopic analysis (NMR, FT-IR, and mass spectrometry) and comparison with literature data. The structure of isolated compounds were *O*-*α*-D-Glc*p*-(1 → 2)-*O*-*β*-D-Fru*f*-(3 → 1)-*O*-*myo*-inositol (**1**), *O*-*α*-D-Glc*p*-(1 → 2)-*O*-*β*-D-Fru*f*-(3 → 1)-*O*-*epi*-inositol (**2**), *O*-*β*-D-Fru*f*-(2 → 6)-*O*-*α*-D-Glc*p*-(1 → 1)-*O*-*β*-D-Glc*p* (**3**), *O*-*β*-D-Fru*f*-(2 → 6)-*O*-α-D-Glc*p*-(1 → 1)-*O*-*β*-D-Gal*p* (**4**), *O*-*β*-D-Fru*f*-(2 → 6)-*O*-*β*-D-Fru*f*-(2 → 6)-*O*-*α*-D-Glc*p*-(1 → 1)-*O*-*β*-D-Glc*p* (**5**), *O*-*β*-D-Fru*f*-(2 → 6)-[*O*-*β*-D-Glc*p*-(1 → 4)]-*O*-*α*-D-Glc*p*-(1 → 1)-*O*-*β*-D-Glc*p* (**6**), *O*-*β*-D-Fru*f*-(2 → 6)-[*O*-*β*-D-Glc*p*-(1 → 4)]-3-OCH_3-*O*-*α*-D-Glc*p*-(1 → 1)-*O*-*β*-D-Glc*p* (**7**), and *O*-*β*-D-Fru*f*-(2 → 6)-[*O*-*β*-D-Glc*p*-(1 → 4)]-*O*-*α*-D-Glc*p*-(1 → 4)-*O*-*α*-D-Glc*p*-(1 → 2)-O-*β*-D-Fru*f* (**8**). The antimicrobial activities of all the isolated compounds (**1**–**8**) were investigated against six microorganisms. Compounds **2** and **3** were effective against *Mycobacterium smegmatis* at minimum inhibitory concentrations (MICs) of 3.13 μg/mL and 3.44 μg/mL, respectively, compared with streptomycin (MIC = 4.0 μg/mL). The enzyme-inhibitory properties of the isolated compounds (**1**–**8**) were evaluated against tyrosinase and *α*-glucosidase. Among the tested compounds, **4** (39.78 ± 10.29 %) exhibited inhibitory activity against tyrosinase, while compound **2** (68.04 ± 4.68 %) exhibited inhibitory activity against α-glucosidase. *In silico* studies of **1**–**8** showed the best predicted binding affinities for the Trehalose-LpqY complex in the range of −11.088 kcal/mol to −14.297 kcal/mol, compared to streptomycin (−6.638 kcal/mol). Compounds **1**–**8** exhibited almost no cytotoxic activity against L-929 cells, further supporting their potential for therapeutic use.

1. Introduction

The genus *Scorzonera* L. is widely distributed across Eurasia and Africa, belongs to the Asteraceae family, and comprises 180 species worldwide [1]. More than 50 species of the *genus Scorzonera* grow in Türkiye, of which 32 are endemic [2–4]. As a significant center of plant diversity, Türkiye hosts a wide variety of *Scorzonera* species, many of which are traditionally consumed as vegetables. Some *Scorzonera* species are traditionally used as a manger in Eastern Anatolia. *Scorzonera mollis* Bieb, known as goftigoda, *Scorzonera suberosa* C. Koch known as

* Corresponding author.
** Corresponding author.
E-mail addresses: yayli@ktu.edu.tr (N. Yaylı), gozdekilic@ktu.edu.tr (G. Bozdal).

https://doi.org/10.1016/j.carres.2026.109833
Received 10 November 2025; Received in revised form 2 January 2026; Accepted 15 January 2026
Available online 16 January 2026
0008-6215/© 2026 Published by Elsevier Ltd.

wild carrot, *Scorzonera cana* (C. A. Meyer) Hoffm. and *Scorzonera latifolia* (Fisch. Et Mey.) DC, also known as mesdek or broadleaf square root, is an edible plant [1,5]. In addition to their edible properties, some *Scorzonera* species have been used in folk medicine across Eurasia [6]. *Scorzonera* is used in Turkish folk medicine for hypertension, arteriosclerosis, diabetes, kidney diseases, and rheumatism [7]. The root of *Scorzonera. tomentosa* L. contains latex, and both the latex and the roots have wound-healing activity [8]. *S. latifolia* is another species that is used in Turkish folk medicine. A gum called 'yakı' is obtained from the latex of this plant and is used for its analgesic and anthelmintic properties, which may help alleviate infertility [3,7]. *Scorzonera pseudodivaricata* Lipsch is used to treat diarrhea, pulmonary edema, and parasitic diseases, and exhibits diuretic and antipyretic effects [5]. *Scorzonera radiata* Fisch. is used in Mongolian folk medicine to treat ulcers and viral infections accompanied by fever, because of its diuretic and galactagogue properties [9]. *S. hispanica* L. has been used as a mucolytic, diuretic, and antipyretic agent, as well as a vegetable, in the treatment of stomach and certain lung diseases, and as a herbal remedy. *Scorzonera mongolica* Maxim. and *Scorzonera austriaca* Willd. They are used as antipyretic and anti-inflammatory agents in traditional Chinese and Tibetan medicine to treat mastitis and abscesses [10]. *Scorzonera humilis* L. has been used to treat wounds and gastrointestinal disorders in Central Europe [10,11].

Various natural compounds, including sesquiterpene lactones, lignans, stilbenoids, triterpenoids, flavonoids, caffeoylquinic acids, and coumarins, have been reported in some *Scorzonera* species [12–16]. Carbohydrates are the major polar components of natural resources. Therefore, the isolation of new carbohydrates in plants is important for food technology. Several oligosaccharides have been identified, including all positional isomers of α- and β-glucobioses, as well as others [17–22]. Oligosaccharides are purported to benefit human health by promoting the growth of bifidobacteria in the large intestine [23]. The structures of oligosaccharides reported to date range from dimers to pentamers. Depending on the biological origin of the oligosaccharide, different linkages between the Glc, Gal, and Fru units have been identified [23–28].

In the phytochemical analyses of *S. yildirimlii* A. Duran & Hamzaoğlu and *S. zorkunensis* Coşkunçelebi & Makbul [2,29], eight new oligosaccharides were isolated and characterized using nuclear magnetic resonance (NMR) spectroscopy and LC-QTOF mass spectrometry. Antimicrobial activities, enzyme inhibition, and *in silico* studies of all isolated compounds (**1**–**8**) were evaluated. Additionally, the cytotoxicity of **1**–**4** against L-929 cells was examined.

2. Materials and methods

2.1. Plant materials

S. yildirimlii and *S. zorkunensis* are endemic species collected from Osmaniye, Türkiye: Zorkun Plateau, Keldaz Hill, 2075 m, on August 20th, 2023. The plants were classified according to the Flora of Turkey [2,30]. *S. yildirimlii* and *S. zorkunensis* were stored in the Karadeniz Technical University (KTU) Department of Biology herbarium (KTUB) under the codes KTUB-242 and KTUB-243, respectively. The whole plants were cleaned, dried in the shade, ground in a mill, and stored in a plastic bag at room temperature until extraction.

2.2. Chemicals, chromatographic, and instrumental methods

All solvents and chemicals were purchased from Sigma-Aldrich. FT-IR (ATR) spectra (4000-400 cm^{-1}) were obtained using a PerkinElmer 1600 spectrometer. The UV spectra were obtained using a Spectrostar Nano BMG Labtech spectrometer. Optical activity was measured using an AA-5 series polarimeter. The melting points were determined using a microscope-type Thermo-var apparatus and were uncorrected. Mass spectra were obtained using an Agilent 6230A high-resolution electron spray ionization mass spectrometry (HRESI-MS). NMR spectra (1D and 2D) were obtained using a Bruker 400/100 MHz NMR spectrometer using CD_3OD and D_2O NMR solvents. The purity of the compounds was determined using a Shimadzu Prominence series HPLC instrument. The Advanced Chemistry Development (ACD) NMR software was used to elucidate the structures of the isolated compounds. Chemical shift values are expressed in δ (ppm). The coupling constants (J) are given in hertz (Hz). Silica gel (Kieselgel 60, 320–400 mesh), Sephadex, and RP-C18 were used for column chromatography. Thin-layer chromatography (TLC) was performed on silica gel plates (Kieselgel 60 F254, Merck). UV (254 nm, 366 nm) and vanillin (0.5 g) were used as markers, along with sulfuric acid and ethanol (80:20). The plates were then heated to 110 °C on a hot plate. The Thermo Scientific Multiskan™ Go Microplate Spectrophotometer was used in enzyme inhibition studies.

2.3. Extraction and isolation

Blended whole parts of *S. yildirimlii* (SY,1118 g, dry) and *S. zorkunensis* (SZ,1250 g, dry) were extracted with methanol (5L x 4, 24 h) at room temperature by maceration. The extracts were filtered, and the solvents were evaporated under vacuum using a rotary evaporator at 40 °C to yield crude methanol extracts (69.21 g (SY), 77.17 g (SZ)). The methanol extracts (67.81 g (SY) and 75.79 g (SZ)) were suspended in H_2O:MeOH (100 mL, 9:1) using an ultrasonic bath and fractionated with *n*-hexane (100 mL x 5; 25.37 g (SYH); 24.91g (SZH), ethyl acetate (100 mL x 5; 4.40 g (SYE); 5.05 g (SZE)), *n*-butanol (100 mL x 5: 15.40 g (SYB); 9.81 g (SZB)), and water (100 mL; 30.61 g (SYW); 28.10 g (SZW)) to yield crude fractions, respectively.

The *n*-butanol fraction (14.40 g) of *S. yildirimlii* (SYB) was subjected to Silica gel column chromatography (CC) using the increased polarity of the CH_2Cl_2:CH_3OH:H_2O (1600:100:0.0; 2000:200:0; 2250:300:30; 1200:400:45; and 750:500:100) mobile phase to obtain 126 fractions (50–75 ml, each). Following thin-layer chromatography (TLC) analysis, some fractions were combined. SYB-Fr 101–107 was 920 mg, and a portion of it (541 mg) was subjected to Sephadex CC using a methanol mobile phase, yielding 64 fractions (5–8 ml each). After the TLC control, subfraction 13:17 gave the compound **1** (73 mg, R_f: 0.12; *n*-butanol: acetone:water (BAW), 4:2:0.5). SYB-Fr 93–100 was 715 mg, and a part of it (250 mg) was purified by preparative thin layer chromatography (PTLC) (20 × 20 cm 0.5 mm ×5 plates) with CH_3CN:H_2O (6:1) mobile phase to give SYB-Fr 93F which afforded compound **2** (30.5 mg, R_f: 0.2). SYB-Fr 63–92 was 873 mg, a part of it (420 mg) was purified by PTLC (20 × 20 cm 0.5 mm ×5 plates) with BAW (4:2:0.5) mobile phase to give SYB-Fr 63C which afforded compound **5** (R_f: 0.45, 68.3 mg), and SYB-Fr 63E was compound **3** (R_f: 0.33, 22 mg).

The *n*-butanol fraction (8.81 g) of *S. zorkunensis* (SZB) was subjected to Silica gel CC using the increased polarity of the CH_2Cl_2:CH_3OH:H_2O (1600:100:0; 2000:200:0; 2250:300:30; 1200:400:45; and 750:500:100) mobile phase to obtain 124 fractions (50–75 ml, each). After TLC control, five subfractions (SZB 1–5) were obtained. SZB 2 (2.48 g) was subjected to Silica gel using vacuum liquid chromatography (VLC) with the increased polarity of the *n*-hexane (500 mL), *n*-hexane-CH_2Cl_2 (1:1, 500 mL), CH_2Cl_2 (500 mL), CH_2Cl_2-acetone (1:1, 500 mL), acetone (500 mL), acetone- ethyl acetate (1:1, 500 mL), ethyl acetate (500 mL), ethyl acetate-methanol (1:1, 500 mL), and methanol (500 mL) mobile phase to give 19 fractions (250–300 ml, each). After the TLC control, 6 subfractions (SZB 2:1–6) were obtained. SZB 2–3 (1323 mg) was separated on Sephadex CC using methanol as the mobile phase, yielding 23 fractions (6–8 mL each). After the TLC control, subfraction SZB 2-3-S-15:22 (266 mg) was further purified by PTLC (20 × 20 cm 0.5 mm x 4 plates) with BAW (4:1:0.1) mobile phase to give compounds **3** (60.4 mg, R_f: 0.33) and **4** (48 mg, R_f: 0.48).

The SZW fraction (25.10 g) was dissolved in water (60 mL) and extracted with methanol:*n*-butanol:ethyl acetate:water (10:10:30:30, x 4) mobile phase to yield two subfractions SZWE (3.4 g) and SZWW (21.6 g). SZWE (3.4 g) was subjected to Silica gel CC using the increased

polarity of diethyl ether (100 mL), diethyl ether-ethyl acetate (1:1, 100 mL), ethyl acetate (200 mL), and ethyl acetate-methanol (8:2, 200 mL; 7:3, 6:4, 1:1, 100 mL each) mobile phase to give 33 fractions (30–40 ml, each). After TLC control, subfraction SZWE 10 (374 mg) was subjected to Sephadex CC using methanol as the mobile phase, yielding 16 fractions (4–6 mL each). After the TLC control, subfraction SZWE 10-9 and SZWE 10–14 gave compounds **6** (73.4 mg, R_f: 0.25, BAW (4:1:0.1)) and **7** (58.2 mg, R_f: 0.14, BAW (4:1:0.1)), respectively. Subfraction SZWE 11:13 yielded compound **8** (125.2 mg, R_f: 0.16, BAW (4:2:0.5)). SZWE 14 (582 mg) was subjected to Sephadex CC using the methanol mobile phase to obtain 15 fractions (5–6 mL each), and subfraction 11 gave sucrose.

Compound 1: O-α-D-Glucopyranosyl-(1 → 2)-*O-β*-D-fructofuranosyl-(3 → 1)-*O-myo*-inositol {*O-α*-D-Glc*p*-(1 → 2)-*O-β*-D-Fru*f*-(3 → 1)-*O-myo*-inositol}, oily; $[\alpha]_D^{24}$ +62.6 (c 0.0116, CH_3OH); R_f: 0.12 (BAW, 4:2:0.5); FT-IR (ATR, cm^{-1}): 3278 (-OH), 2970, 2870 (-CH), 1643, 1512 (C–C), 1056 (C–O); (−) LC-QTOF-MS (*m/z*, %): $C_{18}H_{32}O_{16}$ (504.169 g/mol), $[M-H]^-$ 503.169 (2), calc. 506.162; $[M-2H_2O+K-H]^-$ 506.202 (100), calc. 506.195; $[M+2Na+K+2H]^-$ 591.267 (42), calc. 591.129; $[M+3Na+2H]^-$ 575.267 (18), calc. 575.154; $[M+K]^-$ 543.245 (25), calc. 543.158; $[M+16]^-$ 520.216 (20), calc. 520.164; $[M-Glc]^-$ 341.110 (100), calc. 341.113; ^1H and ^{13}C NMR data presented in Table 1.

Compound 2: O-α-D-Glucopyranosyl-(1 → 2)-*O-β*-D-fructofuranosyl-(3 → 1)-*O-epi*-inositol {*O-α*-D-Glc*p*-(1 → 2)-*O-β*-D-Fru*f*-(3 → 3)-*O-epi*-inositol}, oily; $[\alpha]_D^{24}$ +47.3 (c 0.0264, CH_3OH); R_f: 0.2 (CH_3CN–H_2O, 6:1); FT-IR (ATR, cm^{-1}): 3302 (-OH), 2970, 2870 (-CH), 1643, 1458 (C–C), 1056 (C–O); (−) LC-QTOF-MS (*m/z*, %): $C_{18}H_{32}O_{16}$ (504.169 g/mol), $[M-2H+CH_3OH]^-$ 534.179 (100), calc. 534.234; [M-inositol+2Na]$^-$ 387.106 (45), calc. 387.114; $[Glc+2K-3H]^-$ 255.233 (25), calc. 255.238; ^1H and ^{13}C NMR data presented in Table 1.

Compound 3: O-β-D-Fructofuranosyl-(2 → 6)-*O-α*-D-glucopyranosyl-(1 → 1)-*O-β*-D-glucopyranoside {*O-β*-D-Fru*f*-(2 → 6)-*O-α*-D-Glc*p*-(1 → 1)-*O-β*-D-Glc*p*}, oily; $[\alpha]_D^{24}$ +46.9 (c 0.0358, CH_3OH); R_f: 0.33 (BAW, 4:1:0.1); FT-IR (ATR, cm^{-1}): 3278 (-OH), 2970, 2870 (-CH), 1643, 1458 (C–C), 1056 (C–O); (−) LC-QTOF-MS (*m/z*, %): $C_{18}H_{32}O_{16}$ (504.169 g/mol), $[M-H]^-$ 503.158 (1), calc. 506.162; $[M+Na+K-2H]^-$ 568.188 (100), calc. 568.182; ^1H and ^{13}C NMR data presented in Table 2.

Compound 4: O-β-D-Fructofuranosyl-(2 → 6)-*O*-α-D-glucopyranosyl-(1 → 1)-*O-β*-D-galactopyranoside {*O-β*-D-Fru*f*-(2 → 6)-*O*-α-D-Glc*p*-(1 → 1)-*O-β*-D-Gal*p*}; oily; $[\alpha]_D^{24}$ +51.3 (c 0.0276, CH_3OH); R_f: 0.48 (BAW, 4:1:0.1); FT-IR (ATR, cm^{-1}): 3332 (-OH), 2931, 2890 (-CH), 1643, 1512 (C–C), 1057 (C–O); (−) LC-QTOF-MS (*m/z*, %): $C_{18}H_{32}O_{16}$ (504.169 g/mol), $[M-H]^-$ 503.164 (1), calc. 506.162; $[M+2H_2O-H]^-$ 539.506 (100), calc. 539.183; $[M-CH_2OH+K-H]^-$ 511.475 (90), calc. 511.189; $[M-2OH+K+2H]^-$ 511.475 (90), calc. 511.132; $[M-H_2O+Na+2H]^-$ 511.475 (90), calc. 511.164; ^1H and ^{13}C NMR data see Table 2.

Compound 5: O-β-D-Fructofuranosyl-(2 → 6)-*O-β*-D-fructofuranosyl-(2 → 6)-*O-α*-D-glucopyranosyl-(1 → 1)-*O-β*-D-glucopyranoside {*O-β*-D-Fru*f*-(2 → 6)-*O-β*-D-Fru*f*-(2 → 6)-*O-α*-D-Glc*p*-(1 → 1)-*O-β*-D-Glc*p*}, oily; $[\alpha]_D^{24}$ +9.78 (c 0.1384, CH_3OH); R_f: 0.45 (BAW, 4:2:0.5); FT-IR (ATR, cm^{-1}): 3286 (-OH), 2939, 2868 (-CH), 1643, 1458 (C–C), 1056 (C–O); (−) LC-QTOF-MS (*m/z*, %): $C_{24}H_{42}O_{21}$ (666.221 g/mol), $[M-2H_2O-OH+2H]^-$ 615.195 (20), calc. 615.203; $[M+2CH_3OH]^-$ 730.239 (100), calc. 730.263; $[M-2H_2O+Na]^-$ 653.345 (30), calc. 653.188; ^1H and ^{13}C NMR data presented in Table 2.

Compound 6: O-β-D-Fructofuranosyl-(2 → 6)-[*O-β*-D-glucopyranosyl-(1 → 4)]-*O-α*-D-glucopyranosyl-(1 → 1)-*O-β*-D-Glucopyranoside {*O-β*-D-Fru*f*-(2 → 6)-[*O-β*-D-Glc*p*-(1 → 4)]-*O-α*-D-Glc*p*-(1 → 1)-*O-β*-D-Glc*p*}, oily; $[\alpha]_D^{24}$ +16.6 (c 0.106, CH_3OH); R_f: 0.25 (BAW, 4:1:0.1); FT-IR (ATR, cm^{-1}): 3286 (-OH), 2931, 2885 (-CH), 1643, 1419 (C–C), 1033 (C–O); (−) LC-QTOF-MS (*m/z*, %): $C_{24}H_{42}O_{21}$ (666.221 g/mol), $[M-2H_2O+2K+Na-H]^-$ 730.237 (5), calc. 730.126; $[M+2Na+H_2O]^-$ 730.237 (5), calc. 730.217; $[M-3CH_3OH-2H]^-$ 568.188 (8), calc. 568.135; $[M-Glc-CH_3OH+H_2O-2H]^-$ 435.294 (20), calc. 435.130; $[Glc]^-$ 179.056 (100), calc. 179.056; ^1H and ^{13}C NMR data presented in Table 3.

Compound 7: O-β-D-Fructofuranosyl-(2 → 6)-[*O-β*-D-glucopyranosyl-

Table 1
^1H and ^{13}C NMR data of **1**–**2** (400/100 MHz, CD_3OD, δ in ppm).

		Sucrose	1		2	
		δ_C	δ_C	δ_H (*J* Hz)	δ_C	δ_H (*J* Hz)
α-Glc (1 → 2)	1	92.14	93.90	5.40, 1H, d, 3.8	93.75	5.39, 1H, d, 3.8
	2	71.04	72.42	3.36[a]	72.58	3.40[a]
	3	72.54	74.60	3.87[a]	74.51	3.86[a]
	4	69.19	71.18	3.42[a]	71.40	3.44[a]
	5	72.36	74.63	3.74[a]	74.65	3.75[a]
	6	60.10	62.10	3.75[a], 3.82[a]	62.27	3.72[a], 3.84[a]
β-Fru (2 → 1)	1	61.32	63.46	3.64, bs	63.50	3.60, bs
	2	103.64	105.30	–	105.42	–
	3	76.37	79.12	4.15, d	79.34	4.15, d
	4	73.96	73.08	3.55	73.79	3.58[a]
	5	81.33	83.68	3.78[a]	83.89	3.80[a]
	6	62.34	63.86	3.74[a]	64.09	3.76[a]
myo-inositol (1 → 3)	1		75.61	4.05[a]		
	2,6		74.54	3.94[a]		
	3,5		73.58	3.76[a]		
	4		74.31	3.71[a]		
epi-inositol (1 → 3)	1				75.77	4.04[a]
	2,3,5,6				74.73	3.95[a]
	4				70.09	3.62[a]

[a] Signal patterns are unclear due to overlapping.

Table 2
^1H and ^{13}C NMR data of **3**–**5** (400/100 MHz, CD_3OD, δ in ppm).

		3		4		5	
		δ_C	δ_H (*J* Hz)	δ_C	δ_H (*J* Hz)	δ_C	δ_H (*J* Hz)
β-Fru (2 → 6)	1	62.92	3.68, bs	64.86	3.65, bs	64.27	3.68, bs
	2	99.33	–	99.30	–	99.34	–
β-Fru I (2 → 6)	3	78.18	4.10[a]	78.19	4.08[a]	78.12	4.06[a]
	4	76.93	3.20[a]	76.39	3.22[a]	76.33	3.24[a]
	5	83.35	3.78[a]	83.35	3.79[a]	83.30	3.77[a]
	6	64.65	4.10[a]	64.56	4.16[a]	64.58	3.50[a]
α-Glc (1 → 1)	1	93.94	5.13, 1H, d, 3.8	94.57	5.10, 1H, d,3.6	94.02	5.07, 1H, d, 3.8
	2	71.93	3.32[a]	71.94	3.30[a]	71.89	3.30[a]
	3	74.95	3.40[a]	74.87	3.42[a]	74.92	3.40[a]
	4	71.36	3.70[a]	71.36	3.70[a]	71.77	3.72[a]
	5	73.03	3.80[a]	73.09	3.82[a]	73.07	3.82[a]
	6	65.93	3.50[a], 3.68[a]	65.97	3.52[a], 3.70[a]	65.87	3.50[a], 3.70[a]
β-Glc (1 → 1)	1	98.30	4.49, 1H, d, 7.8			98.25	4.44, 1H, d, 7.8
	2	71.95	3.15, t, 7.8			71.77	3.12, t, 7.8
	3	73.93	3.38[a]			73.87	3.41[a]
	4	69.42	3.70[a]			69.39	3.72[a]
	5	78.15	3.40[a]			77.56	3.44[a]
	6	62.92	3.78[a], 3.86[a]			62.80	3.78[a], 3.88[a]
β-Gal (1 → 1)	1			98.30	4.47, 1H, d, 7.8		
	2			73.09	3.10[a]		
	3			73.94	3.80[a]		
	4			69.46	3.30[a]		
	5			76.84	4.10[a]		
	6			64.33	3.60[a], 3.82[a]		
β-Fru II (2 → 6)	1					62.78	3.70[a]
	2					103.24	–
	3					76.79	4.12[a]
	4					71.30	3.20[a]
	5					84.24	3.78[a]
	6					64.27	4.10[a]

[a] Signal patterns are unclear due to overlapping.

Table 3
^{1}H and ^{13}C NMR data of **6**–**8** (400/100 MHz, D_2O, δ in ppm).

		6		7		8	
		δ_C	δ_H (*J* Hz)	δ_C	δ_H (*J* Hz)	δ_C	δ_H (*J* Hz)
β-Fru (2 → 6)	1	62.43	3.60, bs	62.38	3.60, bs	60.67	3.50[a]
	2	98.04	–	98.06	–	103.58	–
β-Fru I (2 → 6)	3	75.61	4.02[a]	75.85	4.02[a]	73.89	4.05[a]
	4	72.74	3.25[a]	72.65	3.25[a]	71.57	3.26[a]
	5	80.64	3.74[a]	80.57	3.72[a]	81.33	3.76[a]
	6	63.33	3.72[a]	63.27	3.86[a]	62.43	3.60[a]
α-Glc (1 → 1) *α*-Glc I	1	92.06	5.12, 1H, d, 3.7	92.08	5.15, 1H, d, 3.7	92.00	5.28, 1H, d, 3.8
(1 → 1)	2	69.62	3.32[a]	69.56	3.30[a]	69.51	3.42[a]
	3	72.74	3.38[a]	71.97	3.40[a]	70.47	3.60[a]
	4	75.91	3.44[a]	75.85	3.42[a]	70.35	3.64[a]
	5	71.46	3.80[a]	71.37	3.85[a]	72.46	3.80[a]
	6	63.86	3.50[a], 3.74[a]	63.75	3.52[a], 3.72[a]	60.52	3.50[a], 3.62[a]
α-Glc II (1 → 4)	1					92.10	5.16, 1H, d, 3.7
	2					69.59	3.30[a]
	3					71.99	3.46[a]
	4					75.85	3.44[a]
	5					71.57	3.80[a]
	6					63.80	3.45[a], 3.60[a]
β-Glc (1 → 4) *β*-Glc I/ II	1	95.88	4.54, 2H, d, 7.9	95.90	4.56, 2H, d, 7.9	95.81	4.52, 1H, d, 7.9
	2	73.94	3.12, t, 7.9	72.05	3.10, t, 7.8	74.05	3.10, t, 7.9
	3	69.17	3.30[a]	69.10	3.74[a]	69.12	3.68[a]
	4	69.56	3.74[a]	69.48	3.76[a]	67.42	3.75[a]
		67.52	3.60[a]	67.41	3.61[a]		
	5	75.66	3.42[a]	74.02	3.44[a]	75.65	3.42[a]
	6	60.72	3.60[a],	60.63	3.60[a],	60.03	3.62[a],
		60.56	3.82[a]	60.46	3.76[a]		3.84[a]
			3.64[a], 3.80[a]		3.64[a], 3.72[a]		
-OCH_3				55.40	3.62, s		
β-Fru II (2 → 6)	1					62.40	3.70, bs
	2					98.01	–
	3					75.85	3.42[a]
	4					72.68	3.46[a]
	5					80.67	3.75[a]
	6					63.30	3.74[a]

[a] Signal patterns are unclear due to overlapping.

(1 → 4)]-3-OCH_3-*O*-*α*-D-glucopyranosyl-(1 → 1)-*O*-*β*-D-glucopyranoside [O-*β*-D-Fru*f*-(2 → 6)-[O-*β*-D-Glc*p*-(1 → 4)]-3-OCH_3-*O*-*α*-D-Glc*p*-(1 → 1)-O-*β*-D-Glc*p*], oily; $[\alpha]_D^{24}$ +132.7 (c 0.0102, CH_3OH); R_f: 0.14 (BAW, 4:1:0.1); FT-IR (ATR, cm^{-1}): 3363 (-OH), 2970, 2870 (-CH), 1643, 1519 (C–C), 1056 (C–O); (−) LC-QTOF-MS (*m/z*, %): $C_{25}H_{44}O_{21}$ (680.237 g/mol), $[M - H]^-$ 679.510 (1), calc. 679.229; $[M+2Na + K–H]^-$ 764.096 (5), calc. 764.151; $[M\text{-Glc} + CH_3OH]^-$ 533.148 (55), calc. 533.208; ^{1}H and ^{13}C NMR data presented in Table 3.

Compound 8: O-β-D-Fru*f*-(2 → 6)-[*O-β*-D-glucopyranosyl-(1 → 4)]-*O-α*-D-glucopyranosyl-(1 → 4)-*O-α*-D-glucopyranosyl-(1 → 2)-O-*β*-D-fructofuranoside [O-*β*-D-Fru*f*-(2 → 6)-[O-*β*-D-Glc*p*-(1 → 4)]-*O-α*-D-Glc*p*-(1 → 4)-O-*α*-D-Glc*p*-(1 → 2)-O-*β*-D-Fru*f*], oily; $[\alpha]_D^{24}$ +71.4 (c 0.0121, CH_3OH); R_f: 0.16 (BAW, 4:2:0.5); FT-IR (ATR, cm^{-1}): 3332 (-OH), 2924, 2846 (-CH), 1643, 1458 (C–C), 1018 (C–O); (−) LC-QTOF-MS (*m/z*, %): $C_{30}H_{52}O_{26}$ (828.274 g/mol), $[M+3K + Na–H]^-$ 967.421 (20), calc. 967.137; $[M+2Na–H]^-$ 873.448 (5), calc. 873.211; $[M\text{-}2CH_3OH + Na]^-$ 787.357 (85), calc. 787.211; $[M\text{-}2CH_3OH–H_2O–H]^-$ 745.347 (100), calc. 745.214; $[Glc+2K + H_2O–H]^-$ 274.965 (250), calc. 274.996; ^{1}H and ^{13}C NMR data are listed in Table 3.

2.4. HPLC analyses

HPLC chromatographic analyses of **1**–**8** were carried out on a Shimadzu Prominence series HPLC instrument using a Kinetex® C18 (75 mm × 4.6 mm, 2.6 μm) analytical column. The mobile phase was formed of acetonitrile (5 %). The sample injection volume was 10 μL, and the flow rate was 0.8 mL/min. The column furnace temperature was set to 25 °C. The photodiode array detector was operated at 195 nm [31].

2.5. Minimal inhibition concentration (MIC) assay

All microorganisms were purchased from the Hifzissihha Institute of Refik Saydam (Ankara, Türkiye): *Escherichia coli* ATCC35218, *Pseudomonas aeruginosa* ATCC43288, *Staphylococcus aureus* ATCC25923, *Bacillus cereus* 709 Roma, *Mycobacterium smegmatis* ATCC607, and *Candida albicans* ATCC60193. Isolated compound stock solutions were prepared at concentrations ranging from 1000 to 45000 μg/mL. The minimal inhibitory concentration against the test organisms was used to assess antimicrobial activity. Each well received 100 μL of Mueller-Hinton Broth (MHB) or Potato Dextrose Broth (PDB) along with a serially diluted extract solution. Test microorganisms were prepared using a McFarland standard of 0.5 (approximately 1×10^8 cfu/mL) and diluted 1:10. The antimicrobial properties of the *n*-hexane, ethyl acetate, water fractions, methanol extract and compounds **1**–**8** were investigated quantitatively in respective broth media by using triplicate microdilution, and the MIC values (μg/mL) were examined [32,33]. We inoculated each well with 5 μL (equivalent to 5×10^4 cfu) of this dilution. The plates were incubated at 37 °C for 24–48 h. Brain Heart Infusion broth (BHI) (Difco, Detriot, MI) was used for *M. smegmatis* and incubated at 37 °C for 72h. Three independent experiments confirmed the reproducibility of the MIC results. The MIC was defined as the lowest concentration at which no growth was observed. Ampicillin (10 μg/mL), streptomycin (10 μg/mL), and fluconazole (5 μg/mL) were used as the standard antibacterial and antifungal agents. A 1/10 dilution of each solvent was used as the control.

2.6. Enzyme inhibitory properties of compounds

The tyrosinase inhibitory potential of the compounds was determined according to the method described by Ref. [34]. This study reports preliminary screening results at a single concentration (100 μM); IC_{50} values were not determined. Stock solutions of the compounds (10 mM in dimethyl sulfoxide (DMSO)) were diluted with distilled water to obtain working solutions (500 μM). In the study conducted in a 96-well plate, compounds **1**–**8** (100 μM) and the positive control kojic acid (Sigma-Aldrich, K3125) were added to 100 mM phosphate buffer (100 μL, pH 6.8). Then, 20 μL of 500 U/mL tyrosinase (Sigma-Aldrich, T3824) was added to the wells and incubated at room temperature for 15 min. To start with the enzymatic reaction, 3 mM 3,4-dihydroxy-L-phenylalanine (20 μL) (Sigma-Aldrich, D9628) was added as a substrate. After 15 min, the absorbance of the mixtures at 475 nm was measured. The percentage of tyrosinase inhibition by the compounds was calculated using the formula Inhibition (%) = $[(A_0\text{-}A_1)/A_0) \times 100]$. Where A_0 and A_1 represent the absorbance values in the absence and presence of the compounds, respectively. The inhibitory effects of the compound on *α*-glucosidase were determined according to a previously described method with slight modifications [34]. Working solutions (500 μM) were prepared by diluting the stock solutions (10 mM in DMSO) of the compounds with distilled water. Compounds **1**–**8** (100 μM) and the positive control, acarbose (Sigma-Aldrich, A8980), were added to a 96-well plate containing 50 μL phosphate buffer (100 mM, pH 6.8). Then, 100 μL 0.5 U/mL α-glucosidase (Sigma-Aldrich, G5003) was added to each well and incubated at room temperature for 10 min. Subsequently, 50 μL of *p*-nitrophenyl–a–glucopyranoside (Sigma-Aldrich, 487506) (5 mM) solution was added to the wells. After 10 min, the absorbance values of the mixtures at 405 nm were measured using a

microplate reader. α-glucosidase inhibition percentages were calculated as Inhibition (%) = [(A_0-A_1)/A_0) × 100]. Here, A_0 represents the absorbance values in the absence of compounds and A_1 in the presence of compounds.

2.7. Cell viability assay

Compounds **1**–**8** were dissolved in methanol to obtain 50 mg/mL (w/v) stock solutions, which were then diluted to 0.3–100 μg/mL. The cytotoxic effects were evaluated on L-929 mouse fibroblast cells (ATCC®CCL-1™) using the 3-(4,5-dimethylthiazol-2-yl)-2,5-diphenyltetrazolium bromide (MTT) assay (Serva, Germany). L-929 cell line was cultured in high glucose Dulbecco's Modified Eagle's Medium (DMEM) (Wisent, Canada) supplemented with 10 % fetal bovine serum (ATCC, Manassas, USA), 1 % penicillin (100 U/mL), and streptomycin (100 μg/mL) (Wisent, Canada), and maintained at 37 °C in 5 % CO_2 incubator. According to the MTT assay, cells were seeded at 1 × 10^4 cells/well in 96-well plates and incubated for 24 h. The day after plating, the medium was replaced with test chemical solutions (0.1–100 μg/mL) for an additional 24 h. Cells incubated with 0.1 % methanol served as the solvent control. Cells incubated with 3 mM sodium lauryl sulfate (SLS) served as the positive control. Subsequently, the medium was replaced with 100 μL of serum-free medium containing 0.5 mg/mL MTT in each well, and the wells were incubated at 37 °C for 3 h. After that, the MTT-containing medium was gently removed. To dissolve formazan crystals, 150 μL of DMSO was added to each well, and the plate was shaken for 10 min. Absorbance was measured at 570 and 690 nm using a microplate reader (Thermo Scientific, Waltham, MA, USA). The percentage of cell viability was calculated using the following formula: Cell viability % = [(Absorbance of control - Absorbance of treated)/Absorbance of control] × 100 [35].

2.8. Molecular docking procedure

In molecular docking studies, the crystal structure of the Trehalose-LpqY complex (PDB: 7APE), isolated from the *M. thermoresistible* strain, was found to be the most effective for biological activity. In the molecular docking workflow, the protein structure was prepared using the Maestro module in the Schrödinger Small Molecule Drug Discovery Suite (Version 2025-1, Schrödinger, LLC, 2025). For this study, the crystal structure of Trehalose-LpqY, isolated from the *M. thermoresistible* strain [25], was obtained from the Protein Data Bank (PDB). Water molecules in the target protein crystal structure were removed, and the missing atoms in the amino acid structures were subsequently added. In the next step, the hydrogen bonds in the structure were optimized. We applied the OPLS4 force field and carried out energy minimization with a maximum root-mean-square deviation (RMSD) of 0.3 Å (Å). We selected inhibitor compounds associated with enzymes, based on their X-ray crystal structures. We defined a 20 Å grid box surrounding the active sites of the inhibitors using the “receptor grid generation” panel. The OPLS4 force field was utilized again during this stage, with the van der Waals scaling factor set to 0.80 and the charge partial breakpoint set to 0.15 [36]. To validate the molecular docking protocol, the coligand from the X-ray crystal structure of the enzyme was docked into the relevant active site. The resulting conformation then overlapped with the bioactive conformation of the coligand, achieving an RMSD value of 0.1113 Å (Redocking XP Glide score: −12.585 kcal/mol). Three-dimensional structures of the compounds were generated using the Ligprep module. Docking of the compounds to the enzyme active sites was performed using the Extra Precision (XP) algorithm of the Glide module of Schrödinger, on a prerecorded grid file. Three conformations with the lowest glide energies were generated for each compound. Consequently, the predicted binding modes of the compounds at the active sites of the target protein were determined (Table 6 and Fig. 3).

3. Results and discussion

Sugars are a class of carbohydrates that consist of carbon, hydrogen, and oxygen. Carbohydrates serve as an energy source for metabolism. Naturally occurring 1 → 1′, 1 → 2′, 1 → 4′, 2 → 6, and 1 → 6′ linked oligosaccharides have been previously reported [28,37–41]. Oligosaccharides are widely distributed in plants, yeast, algae, lichen, and fungi.

3.1. Chemical structure

The air-dried whole parts of *S. yildirimlii* and *S. zorkunensis* were extracted with methanol and fractionated into *n*-hexane, ethyl acetate, butanol, and water-soluble fractions. The butanol and water fractions were further separated and purified by ordinary-phase chromatography, reversed-phase silica gel chromatography, and Sephadex column chromatography, affording eight compounds (**1**–**8**). The structure of isolated new oligosaccharides **1**–**8**, which are derivatives of sucrose and *α*-*β*-trehalose, was subsequently determined by 1D-NMR (^{1}H, ^{13}C, and attached proton test (APT), 2D-NMR (COSY, HSQC, HMBC, and NOESY) (Tables 1–4), and LC-QTOF mass spectra. All isolated compounds (**1**–**3** and **5** from *S. yildirimlii* and **1**, **3**–**4** and **6**–**8** from *S. zorkunensis*) were elucidated for the first time from *S. yildirimlii* and *S. zorkunensis*. Sucrose was isolated from both species.

Compound **1** was oily, and its molecular formula ($C_{18}H_{32}O_{16}$, 504.169 g/mol) was determined using LC-QTOF-MS, resulting in a molecular ion peak at *m/z* 506.202 (100) [M-2H_2O + K–H]$^-$, with three degrees of unsaturation. The FT-IR spectrum of **1** showed hydroxyl groups at 3278 cm^{-1}, sp^3 hybridized CH at 2970 cm^{-1} and 2870 cm^{-1}, C–C bands at 1643 cm^{-1} and 1512 cm^{-1}, and a C–O–C group at 1056 cm^{-1}. The NMR (^{1}H, ^{13}C/APT, COSY, HSQC, HMBC, and NOESY), FT-IR, and LC-QTOF mass spectra of **1** are available in supplementary data Figs. S1–S9, respectively. The ^{1}H and ^{13}C NMR spectra of **1** showed a single anomeric proton at δ_H 5.40 ppm (d, J = 3.8 Hz) and a carbon peak at δ_C 93.90 ppm (Glc C-1, CH, APT) for the glucose residue. The $^3J_{HH}$ coupling constant (J = 3.8 Hz) between H-1 and H-2 of glucose indicated that the glucosyl bond was of *α* form, as shown in sucrose (Table 1). The ^{1}H NMR spectrum of **1** exhibited a complex pattern in the δ_H range of 3.36–3.87 ppm. ^{1}H COSY and HSQC spectra completed the assignment of all protons and carbons in the *α*-glucose (*α*-Glc*p*) residue (Table 1). The signals at δ_H 4.15 ppm (d, J = 3.8 Hz) showed COSY cross-peaks to H-2, H-3, H-4, H-5, H-6a,b, and exhibited chemical shifts similar to those of the nonreducing residues in **1** (Table 1). An inter-residual HMBC correlation was observed between Glc H-1 (δ_H 5.40 ppm) and Fru C-2 (δ_C 105.30 ppm) (Table 4). The carbon signals at δ_C 93.90 ppm (d, C-1) and δ_C 105.30 ppm (s, C-2) confirmed the presence of glucose and fructose units in **1**, which was identified as a disaccharide. A total of 16 carbons were identified in the ^{13}C/APT and HSQC NMR spectra of **1**, which were characterized as one C, twelve CH, and three CH_2 carbons. Twelve of these were accountable for a sucrose residue of **1**. The remaining four –OCH– peaks at δ_C 75.61 (d, C-1), 74.54 (d, C-2,6), 73.58 (d, C-3,5), and 74.31 (d, C-4) were consistent with the ^{13}C NMR data of inositol, which is a cyclic cyclitol [42]. In the literature, 9 distinct stereoisomers of inositol have been reported, and, depending on their structures, they exhibit one to six carbon signals in the ^{13}C NMR spectrum [43]. Among the naturally occurring inositol compounds, *myo*-inositol has been the most frequently reported. Two di and trigalactosyl-D-*chiro*-inositols have been isolated from *Fagopyrum esculentum* seeds [41]. ^{13}C NMR data for nine inositol derivatives have been reported in the literature [43], and it was observed that the 4-carbon peaks detected for the cyclitol compound **1** matched best with *myo*-inositol [43]. Interglycosidic linkage of inositol was assigned from fructose H-3 (δ_H 4.15 ppm) to the *myo*-inositol C-1 (δ_C 75.61 ppm) based on HMBC correlations [41–43] (Table 4). The NOESY correlation of *α*-Glc*p* H-1 (δ_H 5.40 ppm) to *β*-Fru*f* H-1 (δ_H 3.64 ppm) and *β*-Fru*f* H-3 (δ_H 4.15 ppm) to the *myo*-inositol H-1 (δ_H 4.05 ppm) indicated that *myo*-inositol is linked at the C-3 position of *β*-Fru*f* (Fig. S7) (Table 4). Due to sample limitations, the absolute

Table 4
Long-range H→C and H→H correlation of **1**–**8**.

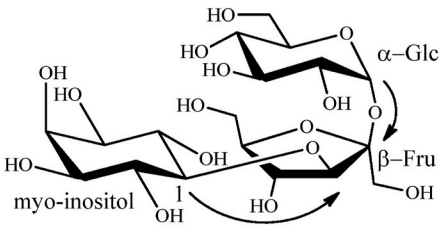
No	HMBC ($^3J_{HC}$)	NOESY
1	*α*-Glc*p* H-1 (δ_H 5.40) to *β*-Fru*f* C-2 (δ_C 105.30) *β*-Fru*f* H-3 (δ_H 4.15) to the *myo*-inositol C-1 (δ_C 75.61)	*α*-Glc*p* H-1 (δ_H 5.40) to *β*-Fru*f* H-1 (δ_H 3.64) and *α*-Glc*p* H-2 (δ_H 3.40) *β*-Fru*f* H-3 (δ_H 4.15) to the *myo*-inositol H-1 (δ_H 4.05)
2	*α*-Glc*p* H-1 (δ_H 5.39) to *β*-Fru*f* C-2 (δ_C 105.42) *β*-Fru*f* H-3 (δ_H 4.15) to the *epi*-inositol C-1 (δ_C 75.77)	*α*-Glc*p* H-1 (δ_H 5.39) to *β*-Fru*f* H-1 (δ_H 3.60) and *α*-Glc*p* H-2 (δ_H 3.40) *β*-Fru*f* H-3 (δ_H 4.15) to the *epi*-inositol H-1 (δ_H 4.04)
3	*α*-Glc*p* H-6a,b (δ_H 3.50, 3.68) to *β*-Fru*f* C-2 (δ_C 99.33) *α*-Glc*p* H-1 (δ_H 5.13) to *α*-Glc*p* C-1 (δ_C 93.94)[a] *β*-Glc*p* H-1 (δ_H 4.49) to *β*-Glc*p* C-1 (δ_C 98.30)[a]	*α*-Glc*p* H-1 (δ_H 5.13 to *β*-Glc H-5 (δ_H 3.40) *β*-Glc*p* H-1 (δ_H 4.49) to *α*-Glc*p* H-2 (δ_H 3.32) and *β*-Glc*p* H-5 (δ_H 3.15) *β*-Fru*f* H-3 (δ_H 4.10) to *β*-Fru*f* H-5 (δ_H 3.78) and *β*-Glc*p* H-4 (δ_H 3.70)
4	*α*-Glc*p* H-6a,b (δ_H 3.52, 3.70) to *β*-Fru*f* C-2 (δ_C 99.30) *α*-Glc*p* H-1 (δ_H 5.10) to *α*-Glc*p* C-1 (δ_C 94.57)[a] *β*-Gal*p* H-1 (δ_H 4.47) to *β*-Gal*p* C-1 (δ_C 98.30)[a]	*α*-Glc*p* H-1 (δ_H 5.10) to *α*-Glc*p* H-2 (δ_H 3.32) *β*-Gal*p* H-1 (δ_H 4.47) to *β*-Glc*p* H-3 (δ_H 3.30) *β*-Fru*f* H-3 (δ_H 4.08) to *β*-Fru*f* H-1(δ_H 3.65)
5	*β*-Fru*f* I H-6 (δ_H 4.10) to *β*-Fru*f* II C-2 (δ_C 103.24) *α*-Glc*p* H-6a,b (δ_H 3.50, 3.68) to *β*-Fru*f* I C-2 (δ_C 99.34) *α*-Glc*p* H-1 (δ_H 5.07) to *α*-Glc*p* C-1 (δ_C 94.02)[a] *β*-Glc*p* H-1 (δ_H 4.44) to *β*-Glc*p* C-1 (δ_C 98.25)[a]	*α*-Glc*p* H-1 (δ_H 5.07) to *α*-Glc*p* H-5 (δ_H 3.44) *β*-Glc*p* H-1 (δ_H 4.44) to *α*-Glc*p* H-2 (δ_H 3.30) *β*-Fru*f* H-3 (δ_H 4.06) to *β*-Fru*f* H-1 (δ_H 3.68)
6	*α*-Glc*p* H-6a,b (δ_H 3.50, 3.74) to *β*-Fru*f* C-2 (δ_C 98.04) *β*-Glc*p* II H-1 (δ_H 4.54) to *α*-Glc*p* C-4 (δ_C 75.91) *α*-Glc*p* H-1 (δ_H 5.12) to *α*-Glc*p* C-4 (δ_C 71.46) *β*-Glc*p* I H-1 (δ_H 4.54) to *β*-Glc*p* I C-4 (δ_C 75.66)	*α*-Glc*p* H-1 (δ_H 5.12) to *β*-Glc*p* I H-5 (δ_H 3.42) *β*-Glc*p* H-1 (δ_H 4.56) to *β*-Glc*p* I H-3 (δ_H 3.30) *β*-Fru*f* H-3 (δ_H 4.02) to *β*-Fru*f* H-1 (δ_H 3.60)
7	*α*-Glc*p* H-6a,b (δ_H 3.52, 3.72) to *β*-Fru*f* C-2 (δ_C 98.06) *β*-Glc*p* II H-1 (δ_H 4.56) to *α*-Glc*p* C-4 (δ_C 75.85) *α*-Glc*p* H-1 (δ_H 5.15) to *α*-Glc*p* C-4 (δ_C 71.37) *β*-Glc*p* I H-1 (δ_H 4.56) to *β*-Glc*p* I C-4 (δ_C 74.02)	*α*-Glc*p* H-1 (δ_H 5.15) to *β*-Glc*p* I H-5 (δ_H 3.44) *β*-Glc*p* H-1 (δ_H 4.56) to *α*-Glc*p* H-3 (δ_H 3.40) and *α*-Glc*p* H-2 (δ_H 3.10) *β*-Fru*f* H-3 (δ_H 4.02) to *β*-Fru*f* H-1 (δ_H 3.60)
8	*α*-Glc*p* II H-6a,b (δ_H 3.45, 3.60) to *β*-Fru*f* II C-2 (δ_C 98.01) *α*-Glc*p* II H-1 (δ_H 5.16) to *α*-Glc*p* I C-4 (δ_C 75.85) *α*-Glc*p* I H-1 (δ_H 5.28) to *β*-Fru*f* I C-2 (δ_C 103.58) *β*-Glc*p* H-1 (δ_H 4.52) to *α*-Glc*p* II C-4 (δ_C 70.35)	*α*-Glc*p* I H-1 (δ_H 5.28) to *β*-Fru*f* I H-1 (δ_H 3.50) and *α*-Glc*p* I H-4 (δ_H 3.64) *α*-Glc*p* II H-1 (δ_H 5.16) to *α*-Glc*p* I H-4 (δ_C 3.44) and *α*-Glc*p* I H-6 (δ_H 3.80) *β*-Glc*p* H-1 (δ_H 4.52) to *α*-Glc*p* II H-3 (δ_H 3.46) and *β*-Glc*p* H-2 (δ_H 3.10) *β*-Fru*f* I H-3 (δ_H 4.05) to *β*-Fru*f* I H-1 (δ_H 3.64)

[a] $^1J_{HC}$ 158–166 Hz.

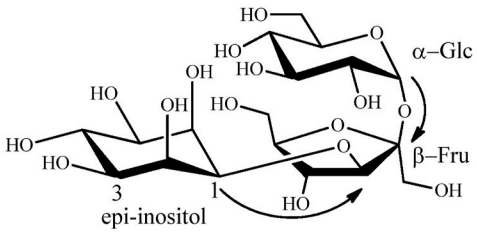
configuration of the inositol moiety was not determined. The proposed configuration is based on a comparison of ^{13}C NMR chemical shifts with literature data [41–43]. The assignments of the carbon peaks obtained from the HSQC and HMBC spectra are presented in Table 1. Consequently, compound **1** was assigned to *O*-*α*-D-Glc*p*-(1 → 2)-*O*-*β*-D-Fru*f*-(3 → 1)-*O*-*myo*-inositol (Fig. 1).

Compound **2** was oily, and its molecular formula ($C_{17}H_{30}O_{15}$, 474.158 g/mol) was determined by LC-QTOF-MS, yielding a molecular ion peak at *m/z* 534.233 [M + Na + K–2H]$^-$, with 3 degrees of unsaturation. The FT-IR spectrum of **2** showed hydroxyl groups at 3302 cm^{-1}, sp^3 hybridized CH at 2970 cm^{-1}and, 2870 cm^{-1}, C–C bands at 1643 cm^{-1} and, 1458 cm^{-1}, and a C–O–C group at 1056 cm^{-1}. The NMR (^{1}H, ^{13}C/APT, COSY, HSQC, HMBC, and NOESY), FT-IR, and LC-QTOF mass spectra of **2** are available in supplementary data Figs. S10–S17, respectively. The ^{1}H and ^{13}C NMR spectra of **2** were similar to those of **1**, suggesting a close relationship with **1**. ^{1}H NMR analysis of **2** showed a single anomeric signal at δ_H 5.39 ppm (d, *J* = 3.8 Hz). ^{13}C/APT NMR spectrum of **2** gave two anomeric carbons at δ_C 93.75 ppm (Gul C-1, d) and 105.42 ppm (Fru C-2, C, s). The signals at δ_H 5.39 ppm were correlated with H-2, H-3, H-4, H-5, and H-6a,b in the COSY spectrum, identifying the *α*-Glc*p* residue. The signals at δ_H 4.15 ppm showed COSY cross-peaks to H-3, H-4, H-5, and H-6, exhibiting chemical shifts resembling those of nonreducing residues in **2** (Table 1). A total of 15 carbons were identified in the ^{13}C/APT and HSQC NMR spectra of **2**, which were characterized as one C, eleven CH, and three CH_2 carbons. The assignment of the carbon peaks for compound **2**, obtained from the HSQC and HMBC spectra, is given in Table 1. A total of 12 carbon signals were assigned at δ_C 93.90 (d, C-1), 72.58 (d, C-2), 74.51 (d, C-3), 71.40 (d, C-4), 74.65 (d, C-5), and 62.27 (t, C-6) for the glucose and peaks at δ_C 63.50 (t, C-1), 105.42 (s, C-2), 79.34 (d, C-3), 75.77 (d, C-4), 83.89 (d, C-5), and 64.09 (t, C-6) for the fructose (Table 1). Twelve of these were accountable for a sucrose residue, as in **1**. HMBC spectra of **2** showed a correlation from Glc H-1 (δ_H 5.39 ppm) to Fru C-2 (δ_C 105.42 ppm). The ^{13}C NMR spectrum of **2** revealed three additional OCH peaks for inositol at δ_C 75.77 (d, C-1), δ_C 74.73 (d, C-2,3,5,6), and δ_C 70.09 (d, C-4) ppm, which were consistent with the ^{13}C NMR data of 3-O-methyl-*epi*-inositol [43]. Since inositol has 9 distinct stereoisomers [42,43], the three observed carbon peaks given above match those of *epi*-inositol [43]. Interglycosidic linkage of inositol was assigned from fructose H-3 (δ_H 4.15 ppm) to the *epi*-inositol C-1 (δ_C 75.61 ppm) based on HMBC correlations [41] (Table 4). The NOESY correlation of *α*-Glc*p* H-1 (δ_H 5.39 ppm) to the *β*-Fru*f* H-1 (δ_H 3.60 ppm) and *β*-Fru*f* H-3 (δ_H 4.15 ppm) to the *epi*-inositol H-1 (δ_H 4.04 ppm) indicated that *epi*-inositol is linked at the C-3 position of *β*-Fru*f* (Fig. S15) (Table 4). Due to sample limitations, the absolute configuration of the inositol moiety was not determined. The proposed configuration is based on a comparison of ^{13}C NMR chemical shifts with literature data [41–43]. Consequently, compound **2** was assigned to *O*-*α*-D-Glc*p*-(1 → 2)-*O*-*β*-D-Fru*f*-(3 → 1)-*O*-*epi*-inositol (Fig. 1).

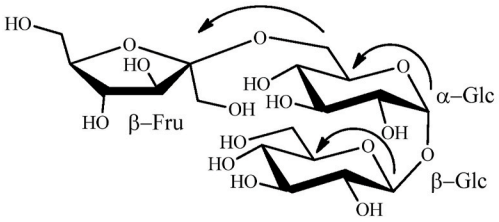
Compound **3** was oily, and its molecular formula ($C_{18}H_{32}O_{16}$, 504.169 g/mol) was determined by LC-QTOF-MS, which yielded a molecular ion peak at *m/z* 568.188 [M + Na + K–2H]$^-$, indicating three degrees of unsaturation. The FT-IR spectrum exhibited absorption bands for hydroxyl groups at 3278 cm^{-1}, sp^3 hybridized CH at 2970 cm^{-1} and 2870 cm^{-1}, C–C bands at 1643 cm^{-1} and 1458 cm^{-1}, and a C–O band at 1056 cm^{-1}. The NMR (^{1}H, ^{13}C/APT, COSY, HSQC, HMBC, and NOESY), FT-IR, and LC-QTOF mass spectra of **3** are available in supplementary data Figs. S18–S26, respectively. The ^{1}H NMR spectrum of **3** showed two anomeric signals at δ_H 5.13 ppm (d, 1H, *J* = 3.8 Hz) and δ_H 4.49 ppm (d, 1H, *J* = 7.8 Hz). The signals at δ_H 5.13 ppm ($^3J_{1,2}$ = 3.8 Hz) and δ_H 4.49 ppm ($^3J_{1,2}$ = 7.8 Hz) showed correlations to H-2, H-3, H-4, H-5, and H-6a,b in the COSY spectrum, identifying the *α*-Glcp and *β*-Glcp residues, respectively. The signals at δ_H 4.10 ppm (Fru H-6) showed COSY cross-peaks to H-5, H-4, and H-3, which are similar to those of the nonreducing residues (Table 2). ^{13}C and APT NMR spectra of **3** allowed the identification of 18 carbon, and the carbon signals at δ_C 93.94 ppm (*α*-, C-1, d), δ_C 98.30 ppm (*β*-, C-1, d), and δ_C 99.33 ppm (C-2, s) confirmed to be a trisaccharide consisting of one *α*-D-glucopyranose, one *β*-D-glucopyranose, and one *β*-D-fructofuranans due to the $^3J_{HH}$ and $^1J_{CH}$ coupling constants, respectively [26]. The assignment of the carbons in **3**, obtained from the HSQC and HMBC spectra, is given in Tables 2 and 4 Two anomeric protons (δ_H 5.13 ppm (d, 1H, 3.8 Hz) and δ_H 4.49 ppm (d, 1H, 7.8 Hz) and carbon signals (δ_C 93.94 ppm, d, *α*-, C-1, δ_C 98.30, d, *β*-, C-1) of glucose units of **3** showed that two glucose units were linked by 1 → 1′ linkage and known as trehalose [26]. The C-1 carbons (δ_C 93.94 ppm and δ_C 98.30 ppm) of *α*-/*β*-glucose showed a $^1J_{HC}$ 166 and 158 Hz (HMBC) coupling, resulting in *α*-D-Glc*p*-(1 → 1)-*O*-*β*-D-Glc*p* [26,37,44,45]. ^{13}C NMR data of C-6 for *α*-D-Glc*p* were shifted downfield at δ_C 65.93 ppm and showed an interglycosidic linkage (HMBC) with *β*-D-Fru*f* (2 → 6). HMBC spectra of **3** showed correlations from *α*-Glc H-6a,b (δ_H 3.50, 3.68 ppm) to Fru C-2 (δ_C 99.33 ppm) (Table 4). Trehalose is a disaccharide with a 1 → 1′ linkage in the *α*,*α*, or *α*,*β*- configuration. All proton and carbon values of compound **3** are consistent with



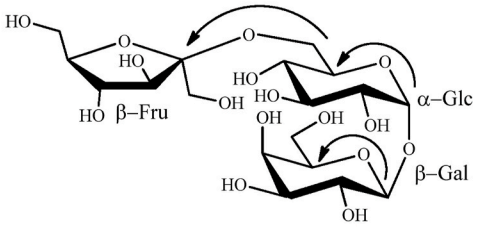
O-*α*-D-Glc*p*-(1→2)-*O*-*β*-D-Fru*f*-(3→1)-*O*-*myo*-inositol (**1**)



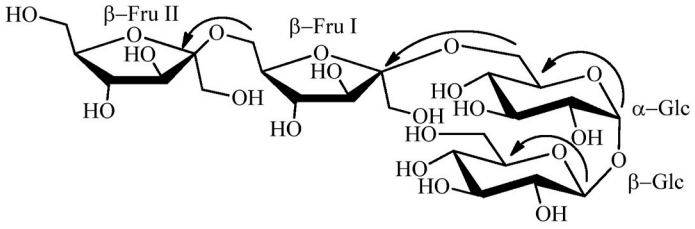
O-*α*-D-Glc*p*-(1→2)-*O*-*β*-D-Fru*f*-(3→1)-*O*-*epi*-inositol (**2**)



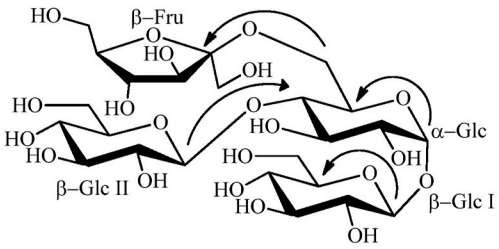
O-*β*-D-Fru*f*-(2→6)-*O*-*α*-D-Glc*p*-(1→1)-*O*-*β*-D-Glc*p* (**3**)



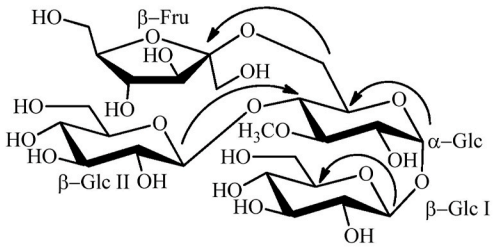
O-*β*-D-Fru*f*-(2→6)-*O*-α-D-Glc*p*-(1→1)-*O*-*β*-D-*Galp* (**4**)



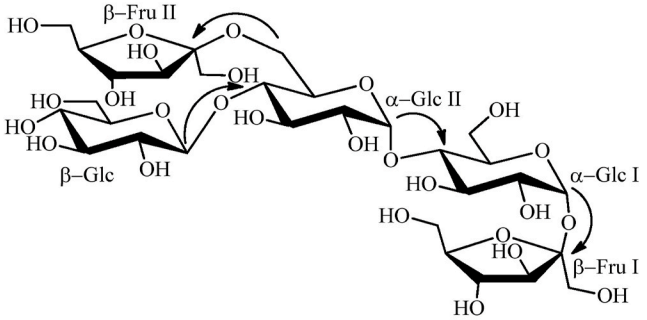
O-*β*-D-Fru*f*-(2→6)-*O*-*β*-D-Fru*f*-(2→6)-*O*-*α*-D-Glc*p*-(1→1)-*O*-*β*-D-Glc*p* (**5**)



O-*β*-D-Fru*f*-(2→6)-[*O*-*β*-D-Glc*p*-(1→4)]-*O*-*α*-D-Glc*p*-(1→1)-*O*-*β*-D-Glc*p* (**6**)



O-*β*-D-Fru*f*-(2→6)-[*O*-*β*-D-Glc*p*-(1→4)]-3-OCH3-*O*-*α*-D-Glc*p*-(1→1)-*O*-*β*-D-Glc*p* (**7**)



O-*β*-D-Fru*f*-(2→6)-[*O*-*β*-D-Glc*p*-(1→4)]-*O*-*α*-D-Glc*p*-(1→4)-*O*-*α*-D-Glc*p*-(1→2)-*O*-*β*-D-Fru*f* (**8**)

HMBC

Fig. 1. Chemical structures of oligosaccharides (**1**–**8**) are isolated from *S. yildirimlii* and *S. zorkunensis*.

α,β-trehalose [26]. HMBC spectra of **3** showed $^{3}J_{CH}$ correlations from the α-Glc H-1 (δ_H 5.13 ppm) to the α-Glc C-3 and C-5 (δ_C 74.95 ppm, δ_C 73.03 ppm) and from the β-Glc H-1 (δ_H 4.49 ppm) to the β-Glc C-5 (δ_C 78.15 ppm). However, no correlation was observed from the α-Glc H-1 to the β-Glc C-1 in the HMBC spectrum. Comparison of NMR data of **3** with the literature, two glucose units in compound **3** are glycosidically bonded via a 1 → 1′ linkage [26,37,44,45]. Compound **3** appears to be an isomer of *O*-β-D-Glc*p*-(1 → 4)-*O*-α-D-Glc*p*-(1 → 2)-*O*-β-D-Fru*f* (cellobiose-Fru) [21]. However, the appearance of the fructose anomeric carbon peak at δ_C 99.00 ppm and the α-Glc C-6 carbon peak at δ_C 65.97 ppm showed that the monosaccharide units were in different sequences [23,26,37,44,45]. The NOESY correlation of α-Glc*p* H-1 (δ_H 5.13 ppm) to the β-Glc H-5 (δ_H 3.40 ppm), β-Glc*p* H-1 (δ_H 4.49 ppm) to the α-Glc*p* H-2 (δ_H 3.32 ppm), and β-Fru*f* H-3 (δ_H 4.10 ppm) to the β-Glc*p* H-4 (δ_H 3.70 ppm) indicated that the trisaccharide is in the linkage of the β-Fru*f*-(2 → 6)-α-Glc*p*-(1 → 1)-β-Glc*p* (Fig. S24) (Table 4). NOESY spectrum of **3** did not show correlation from α-Glcp H-1 to β-Glcp H-1, due to the trans position. This indicated that the H-1 protons of two glucose molecules were in the trans position. Thus, compound **3** was assigned to *O*-β-D-Fru*f*-(2 → 6)-*O*-α-D-Glc*p*-(1 → 1)-*O*-β-D-Glc*p* (Fig. 1). The isomer of **3** is known in the literature as *O*-β-D-Fru*f*-(2 → 6)-*O*-α-D-Glc*p*-(1 → 1)-*O*-α-D-Glc*p* [45].

Compound **4** was oily. Its LC-QTOF-MS showed an $[M+2H_2O–H]^-$ ion peak at *m/z* 539.506 (100), corresponding to the molecular formula $C_{18}H_{32}O_{16}$ and 3 degrees of unsaturation. The FT-IR spectrum of **4** showed hydroxyl groups at 3332 cm^{-1}, sp^3 hybridized CH at 2931 cm^{-1}, 2890 cm^{-1}, C–C bands at 1643 $cm^{-1}$and, 1512 cm^{-1}, and C–O band at 1057 cm^{-1}. The NMR (^{1}H, ^{13}C/APT, COSY, HSQC, HMBC, and NOESY), FT-IR, and LC-QTOF mass spectra of **4** are available in supplementary data Figs. S27–S35, respectively. The structure of **4** was determined using NMR spectroscopy (^{1}H, ^{13}C/APT, HSQC, and HMBC). The ^{1}H and ^{13}C NMR spectra of **4** were similar to those of **3**, suggesting a close relationship with the structure **3**. ^{1}H NMR analysis of **4** showed two anomeric signals at δ_H 5.10 ppm (d, $J = 3.6$ Hz) and δ_H 4.47 ppm (d, $J =$ 7.8 Hz), which correlated with H-2, H-3, H-4, H-5, and H-6a,b in the COSY spectrum, identifying the α-Glc*p* and β-Gal*p* residues, respectively. ^{13}C/APT NMR spectrum of **4** allowed the identification of 18 carbon and the carbon signals and three anomeric carbons at δ_C 94.57 ppm (Gul C-1, d), δ_C 98.30 ppm (Gal C-1, d), and δ_C 99.34 ppm (Fru C-2, C, s) showing the compound **4** is in a trisaccharide (Table 2). Two anomeric protons (δ_H 5.13 ppm (d, 1H, 3.8 Hz) and δ_H 4.49 ppm (d, 1H, 7.8 Hz) and carbon signals (δ_C 94.57 ppm d, α-, C-1, δ_C 98.30, d, β-, C-1) of glucose and galactose showed that they were linked by 1 → 1′ linkage [26]. The C-1 carbons (δ_C 94.57 ppm and δ_C 98.30 ppm) of α-glucose and β-galactose showed a $^1J_{HC}$ 162 and 160 Hz (HMBC) coupling, resulting in α-D-Glc*p*-(1 → 1)-O-β-D-Gal*p* [26]. ^{13}C NMR data of C-6 for α-D-Glc*p* were shifted downfield at δ_C 65.97 ppm and showed an interglycosidic linkage (HMBC) with β-D-Fru*f* (2 → 6). HMBC spectra of **4** showed correlations from α-Glc H-6a,b (δ_H 3.52, 3.70 ppm) to Fru C-2 (δ_C 99.30 ppm), from the α-Glc H-1 (δ_H 5.10 ppm) to the α-Glc C-5 (δ_C 73.09 ppm), and from the β-Gal H-1 (δ_H 4.47 ppm) to the β-Gal C-5 (δ_C 76.84 ppm) (Table 4). However, no correlation was observed from the α-Glc H-1 to the β-Gal C-1 in the HMBC spectrum. Comparison of NMR data of **4** with the literature, glucose and galactose units in compound **4** are glycosidically bonded via a 1 → 1′ linkage [26,37,44,45]. Compound **4** appears to be an isomer of *O*-β-D-Gal*p*-(1 → 4)-*O*-α-D-Glc*p*-(1 → 2)-*O*-β-D-Fru*f* (lactose-Fru) [21]. However, the appearance of the fructose anomeric carbon peak at δ_C 99.30 ppm and the α-Glc C-6 carbon peak at δ_C 65.97 ppm showed that the monosaccharide units were in different sequences [23,26,37,44,45]. The NOESY correlation of α-Glc*p* H-1 (δ_H 5.10) to α-Glc*p* H-2 (δ_H 3.32), β-Gal*p* H-1 (δ_H 4.47) to β-Glc*p* H-3 (δ_H 3.30), and β-Fru*f* H-3 (δ_H 4.08) to β-Fru*f* H- 1 (δ_H 3.65) indicated the trisaccharide as β-Fru*f,* α-Glc*p*, and β-Gal*p* (Fig. S33) (Table 4). NOESY spectrum of **4** did not show correlation from α-Glc*p* H-1 to β-Gal*p* H-1, due to the trans position. This indicated that the H-1 protons of two glucose molecules were in the trans position. Thus, compound **4** was assigned to *O*-β-D-Fru*f*-(2 → 6)-*O*-α-D-Glc*p*-(1 → 1)-*O*-β-D-Gal*p* (Fig. 1).

Compound **5** was oily, and its molecular formula ($C_{24}H_{42}O_{21}$, 666.221 g/mol) was determined by LC-QTOF-MS, which yielded a molecular ion peak at *m/z* $[M + Na + K+2H]^-$ 730.239 (100), corresponding to four degrees of unsaturation. The FT-IR spectrum exhibited absorption bands for hydroxyl groups at 3286 cm^{-1}, sp^3 hybridized CH at 2939 cm^{-1} and 2868 cm^{-1}, C–C bands at 1643 cm^{-1} and 1458 cm^{-1}, and a C–O band at 1056 cm^{-1}. The structure of **5** was determined using NMR (^{1}H, ^{13}C/APT, HSQC, and HMBC) and LC-QTOF mass spectrometry. The NMR (^{1}H, ^{13}C/APT, COSY, HSQC, HMBC, and NOESY), FT-IR, and LC-QTOF mass spectra of **5** are available in supplementary data Figs. S36–S45, respectively. The ^{1}H and ^{13}C NMR spectra of **5** were similar to those of **3**, except for the presence of an additional terminal fructose unit. The ^{1}H NMR spectrum of **5** (Table 2) showed two anomeric proton signals at δ_H 5.07 ppm (d, 1H, 3.8 Hz) and δ_H 4.44 ppm (d, 1H, 7.8 Hz), which were correlated to H-2, H-3, H-4, H-5, and H-6a,b in the COSY spectrum, identifying the α-Glc*p* and β-Glc*p* residue, respectively. The signals at δ_H 4.15 ppm (Fru-I H-6) and δ_H 4.10 ppm (Fru-II H-6) exhibited COSY cross-peaks to H-5, H-4, and H-3, which resembled the chemical shifts of nonreducing residues in **5** (Table 2). The ^{13}C/APT NMR spectrum of **5** allowed the identification of 24 carbon atoms. Four anomeric carbon signals were observed at δ_C 94.02 ppm (α-Glc C-1, d), δ_C 98.25 ppm (β-Glc C-1, d), δ_C 99.34 ppm (Fru I C-2, C, s), and δ_C 103.24 ppm (Fru II C-2, C, s), showing the compound **5** is in a tetrasaccharide structure. Two anomeric protons at δ_H 5.06 ppm (d, 1H, 3.8 Hz) and δ_H 4.44 ppm (d, 1H, 7.8 Hz) and carbon signals of two glucoses at δ_C 94.02 ppm (d, α-, C-1) and δ_C 98.25 ppm (d, β-, C-1) showed that they were linked by 1 → 1′ linkage [26,37,44,45]. The C-1 carbons (δ_C 94.02 ppm and δ_C 98.25 ppm) of α-/β-glucose showed a $^1J_{HC}$ 162 and 158 Hz (HMBC) coupling, resulting in α-D-Glc*p*-(1 → 1′)-*O*-β-D-Glc*p* [26,37,44]. ^{13}C NMR data of C-6 for α-D-Glc*p* were shifted downfield at δ_C 65.97 ppm, and HMBC spectra of **5** showed an interglycosidic linkage from α-D-Glc H-6 (δ_H 3.50, 3.70 ppm) to the β-D-Fru*f* I C-2 (δ_C 99.34 ppm) and from Fru I H-6 (δ_H 3.50 ppm) to Fru II C-2 (δ_C 103.24 ppm), showing the 2 → 6 linkages. HMBC spectra of **5** showed $^{3}J_{CH}$ correlations from the α-Glc H-1 (δ_H 5.07 ppm) to the α-Glc C-5 (δ_C 73.07 ppm) and from the β-Glc H-1 (δ_H 4.44 ppm) to the β-Glc C-5 (δ_C 77.56 ppm) (Table 4). However, no correlation was observed from the α-Glc H-1 to the β-Glc C-1 in the HMBC spectrum. Comparison of the NMR data for **5** with the literature, two glucose units (α/β) in compound **5** are glycosidically linked via a 1 → 1′ as in **3** [26,37,44,45]. The NOESY correlation of α-Glc*p* H-1 (δ_H 5.07 ppm) to the β-Glc H-5 (δ_H 3.44 ppm), β-Glc*p* H-1 (δ_H 4.44 ppm) to the α-Glc*p* H-2 (δ_H 3.30 ppm), and β-Fru*f* H-3 (δ_H 4.06 ppm) to the β-Fru*f* H-1 (δ_H 3.68 ppm) indicated that part of compound **5** is in the linkage of the β-Fru*f* I-(2 → 6)-α-Glc*p*-(1 → 1)-β-Glc*p* (Fig. S43) (Table 4). NOESY spectrum of **5** did not show correlation from α-Glc*p* I H-1 to β-Glc*p* I H-1, due to the trans position. This indicated that the H-1 protons of two glucose molecules were in the trans position. Consequently, compound **5** was assigned to a linear structure as *O*-β-D-Fru*f*-(2 → 6)-*O*-β-D-Fru*f*-(2 → 6)-*O*-α-D-Glc*p*-(1 → 1)-*O*-β-D-Glc*p* (Fig. 1).

Compound **6** was oily. Its LC-QTOF-MS showed a $[M-2H_2O+2K + Na–H]^-$ or $[M+2Na + H_2O]^-$ ion peak at *m/z* 730.237 (5), corresponding to a molecular formula of $C_{24}H_{42}O_{21}$ (666.221 g/mol) with four degrees of unsaturation. The FT-IR spectrum of **6** showed hydroxyl groups at 3286 cm^{-1}, sp^3 hybridized CH at 2931 $cm^{-1}$and, 2885 cm^{-1}, C–C bands at 1643 $cm^{-1}$and, 1419 cm^{-1}, and a C–O–C group at 1033 cm^{-1}. The structure of **6** was determined using NMR (^{1}H, ^{13}C/APT, HSQC, and HMBC) and LC-QTOF mass spectrometry. The NMR (^{1}H, ^{13}C/APT, COSY, HSQC, HMBC, and NOESY), FT-IR, and LC-QTOF mass spectra of **6** are available in supplementary data Figs. S46–S56, respectively. ^{1}H and ^{13}C NMR spectra of **6** were similar to the NMR data of **3,** except for an additional glucose inter-unit. The ^{1}H NMR spectrum of **6** (Table 3) showed three anomeric proton signals at δ_H 5.12 ppm (d, 1H, 3.7 Hz) and δ_H 4.54 ppm (d, 2H, 7.9 Hz) and had correlations to H-2, H-3, H-4, H-5, and H-6a,b in the COSY spectrum, identifying the α-Glc*p* and two

β-Glc*p* residues, respectively. Two proton peaks integrated at δ_H 4.54 ppm seen in the proton NMR spectrum of **5** indicate the presence of two glucose molecules and coincide with the chemical values of the anomeric proton peaks of cellobiose *O*-β-D-Glc*p* (δ_H 4.48 ppm, d, 7.8) [21] and α, β-trehalose *O*-β-D-Glc*p* (δ_H 4.65 ppm, d, 7.8) [44]. The signals at δ_H 3.72 ppm (Fru H-6) showed COSY cross-peaks to H-5, H-4, and H-3, which are similar to those of the nonreducing residue in **6** (Table 3). ^{13}C/APT NMR spectrum of **6** allowed for the identification of 20 carbon atoms, and some carbon peaks were overlapped. Four anomeric carbon signals were observed at δ_C 92.06 ppm (α-Gul C-1, d), δ_C 95.88 ppm (2x β-Glc I and II C-1, d), and δ_C 98.04 ppm (Fru C-2, C, s), showing that compound **6** is in a tetrasaccharide structure (Table 3). Two anomeric protons (δ_H 5.12 ppm (d, 1H, 3.7 Hz) and δ_H 4.54 ppm (d, 2H, 7.9 Hz) and carbon signals (α-Glc, δ_C 92.06 ppm, d, C-1; β-Glc I, δ_C 95.88, d, C-1 x 2) of two glucoses showed that they were linked by 1 → 1′ linkage. Carbon chemical shifts and coupling of α-Glc and β-Glc ($^1J_{1,2}$ 162 and 158 Hz, HMBC) resulted in the formation of α-D-Glc*p*-(1 → 1)-*O*-β-D-Glc*p* I [26,37,44]. ^{13}C NMR data of **6** showed that the C-6 carbon peak for the α-D-Glc*p* was shifted downfield at δ_C 63.86 ppm and showed a terminal glycoside linkage (HMBC) with C-2 of β-D-Fru*f*. Interglycosidic linkage of β-D-Glc*p* II was assigned from β-D-Glc*p* II H-1 (δ_H 4.54 ppm) to α-D-Glc*p* C-4 (δ_C 75.91 ppm) based on HMBC correlations [23,46] (Table 4). HMBC spectra of **6** showed correlations similar to those of compound **3** (Table 4). However, no correlation was observed from the α-Glc H-1 to the β-Glc I C-1 in the HMBC spectrum. Comparison of NMR data of **6** with the literature, two glucose units (α/β) in compound **6** are linked by a 1 → 1′ linkage [26,37,44,45]. The NOESY correlation of α-Glc*p* H-1 (δ_H 5.12 ppm) to the β-Glc*p* I H-5 (δ_H 3.42 ppm), β-Glc*p* H-1 (δ_H 4.56 ppm) to the β-Glc*p* I H-3 (δ_H 3.30 ppm), and β-Fru*f* H-3 (δ_H 4.02 ppm) to the β-Fru*f* H-1 (δ_H 3.60 ppm) indicated that part of compound **6** is in the linkage of the [β-Glc*p* II-(1 → 4)]-α-Glc*p*-(1 → 1)-β-Glc*p* I (Fig. S54) (Table 4). NOESY spectrum of **6** did not show correlation from α-Glc*p* H-1 to β-Glc*p* I H-1, due to the trans position. This indicated that the H-1 protons of two glucose molecules were in the trans position. Thus, compound **6** was assigned to *O*-β-D-Fru*f*-(2 → 6)-[*O*-β-D-Glc*p*-(1 → 4)]-*O*-α-D-Glc*p*-(1 → 1)-*O*-β-D-Glc*p* (Fig. 1).

Compound **7** was oily, and its molecular formula ($C_{25}H_{44}O_{21}$, 680.237 g/mol) was assigned by LC-QTOF-MS, which yielded a molecular ion peak at *m/z* [M+2Na + K–H]$^-$ 764.096 (5), corresponding to four degrees of unsaturation. The FT-IR spectrum of **7** showed hydroxyl groups at 3363 cm^{-1}, sp^3 hybridized CH at 2970 cm^{-1} and, 2870 cm^{-1}, C–C bands at 1643 cm^{-1}and, 1519 cm^{-1}, and a C–O–C group at 1056 cm^{-1}. NMR (^{1}H, ^{13}C/APT, COSY, HSQC, HMBC, and NOESY), FT-IR, and LC-QTOF mass spectra of **7** are shown in Supplementary data Figs. S57–S66, respectively. The ^{1}H and ^{13}C NMR spectra of **7** are similar to those of **6**, except for the presence of an additional methoxy group. The ^{1}H NMR spectrum of **7** (Table 3) showed three anomeric proton signals at δ_H 5.12 ppm (d, 1H, 3.7 Hz) and δ_H 4.54 ppm (d, 2H, 7.9 Hz) and had correlations to H-2, H-3, H-4, H-5, and H-6a,b in the COSY spectrum, identifying the α-Glc*p* and two β-Glc*p* residues, respectively. The signals at δ_H 3.74 ppm (Fru H-6) showed COSY cross-peaks to H-5, H-4, and H-3, assignable to β-Fru*f* (Table 3). The ^{1}H NMR spectrum showed a single methoxy group at δ_H 3.62 ppm (s, 3H). ^{13}C/APT NMR spectrum of **7** allowed for the identification of 21 carbon atoms, and some carbon peaks overlapped. Four anomeric carbon signals were observed at δ_C 92.08 ppm (α-Gul C-1, d), δ_C 95.90 ppm (2 × β-Glc I and II C-1, d), and δ_C 98.06 ppm (Fru C-2, C, s), indicating that compound **7** is part of a tetrasaccharide structure. The two anomeric protons, at δ_H 5.15 ppm (d, 1H, 3.7 Hz) and δ_H 4.56 ppm (d, 2H, 7.9 Hz), and the anomeric carbon signals of the two glucose units indicated that they were linked by a 1 → 1′ linkage [26,37,44,45]. Carbon chemical shifts and coupling of α-Glc and β-Glc I ($^1J_{HC}$ 162 and 158 Hz, HMBC) resulted in α-D-Glc*p*-(1 → 1)-*O*-β-D-Glc*p*-I [26,37,44]. ^{13}C NMR data of C-6 for α-D-Glc*p* was shifted downfield at δ_C 63.75 ppm and showed a terminal glycoside linkage (HMBC) with C-2 of β-D-Fru*f*. Interglycosidic linkage of β-D-Glc*p* was assigned from β-D-Glc*p* II C-1 (δ_H 4.40 ppm) and α-D-Glc*p* C-4 (δ_C 75.85 ppm) based on HMBC correlations [23,27,46] (Table 4). The methoxy proton peak at δ_H 3.62 ppm showed an HMBC correlation with α-D-Glc*p* C-3 (δ_C 71.97 ppm) [23,27,46]. The NOESY correlation of α-Glc*p* I H-1 (δ_H 5.15 ppm) to the β-Glc*p* I H-5 (δ_H 3.44 ppm), β-Glc*p* H-1 (δ_H 4.56 ppm) to the α-Glc*p* H-3 (δ_H 3.30 ppm), and β-Fru*f* H-3 (δ_H 4.02 ppm) to the β-Fru*f* H-1 (δ_H 3.60 ppm) indicated that part of compound **7** is in the linkage of the [β-Glc*p* II-(1 → 4)]-α-Glc*p*-(1 → 1)-β-Glc*p* I (Fig. S64) (Table 4). NOESY spectrum of **7** did not show correlation from α-Glc*p* H-1 to β-Glc*p* I H-1, due to the trans position. This indicated that the H-1 protons of two glucose molecules were in the trans position. Consequently, compound **7** was assigned to *O*-β-D-Fru*f*-(2 → 6)-[*O*-β-D-Glc*p*-(1 → 4)]-3-OCH$_3$-*O*-α-D-Glc*p*-(1 → 1)-*O*-β-D-Glc*p* (Fig. 1).

Compound **8** was oily, and its molecular formula ($C_{30}H_{52}O_{26}$, 828.274 g/mol) was determined by LC-QTOF-MS, which yielded a molecular ion peak at *m/z* 873.448 (10) [M+2Na–H]$^-$, with 5 degrees of unsaturation. The FT-IR spectrum of **8** exhibited an absorption band for the hydroxyl group at 3332 cm^{-1}, sp^3 hybridized CH at 2924 cm^{-1}, 2846 cm^{-1}, C–C bands at 1643 cm^{-1} and 1458 cm^{-1}, and a C–O–C group at 1018 cm^{-1}. The structure of **8** was determined using NMR (^{1}H, ^{13}C/APT, HSQC, and HMBC) and LC-QTOF mass spectra. The NMR (^{1}H, ^{13}C/APT, COSY, HSQC, HMBC, and NOESY), FT-IR, and HR-ESI-MS spectra of **8** are available in supplementary data Figs. S67–S77, respectively. A portion of the ^{1}H and ^{13}C NMR data of **8** was similar to the NMR data of **6**, except for the presence of an additional terminal sucrose unit. The ^{1}H NMR spectrum of **8** (Table 3) showed three anomeric proton signals at δ_H 5.28 ppm (d, 1H, 3.8 Hz), δ_H 5.16 ppm (d, 1H, 3.7 Hz), and δ_H 4.52 ppm (d, 2H, 7.9 Hz) and had correlations to H-2, H-3, H-4, H-5, and H-6a,b in the COSY spectrum, identifying the two different α-D-Glc*p* and one β-D-Glc*p* residue, respectively. The signals at δ_H 3.74 ppm (Fru II H-6) and δ_H 3.60 ppm (Fru I H-6) exhibited COSY cross-peaks to H-5, H-4, and H-3, which resemble the chemical shifts of both terminal non-reducing residues in **8** (Table 3). ^{13}C/APT NMR spectrum of **8** allowed the identification of 30 carbon atoms. Five anomeric carbon signals were observed at δ_C 92.10 ppm (α-Gul I C-1, d), δ_C 92.00 ppm (α-Gul II C-1, d), δ_C 95.81 ppm (β-Glc, C-1, d), δ_C 98.01 ppm (Fru II C-2, C, s), and δ_C 103.58 ppm (Fru I C-2, C, s), showing that the compound **8** is in a pentasaccharide structure (Table 3). ^{13}C NMR data of **8** revealed that the α-D-Glc*p* II C-6 carbon signal at δ_C 63.80 ppm was shifted downfield, indicating a glycoside linkage. HMBC correlations of **8** were observed from α-Glc*p* II H-6a,b (δ_H 3.45, 3.60 ppm) to β-Fru*f* II C-2 (δ_C 98.01 ppm), from α-Glc*p* II H-1 (δ_H 5.16 ppm) to α-Glc*p* I C-4 (δ_C 75.85 ppm), from α-Glc*p* I H-1 (δ_H 5.28 ppm) to β-Fru*f* I C-2 (δ_C 103.58 ppm), and from β-Glc*p* H-1 (δ_H 4.52 ppm) to α-Glc*p* II C-4 (δ_C 70.35 ppm) [27,46,47] (Table 4). The NOESY correlation of α-Glc*p* I H-1 (δ_H 5.28 ppm) to β-Fru*f* I H-1 (δ_H 3.50 ppm), α-Glc*p* II H-1 (δ_H 5.16 ppm) to α-Glc*p* I H-4 (δ_C 3.44 ppm), and β-Glc*p* H-1 (δ_H 4.52 ppm) to α-Glc*p* II H-3 (δ_H 3.46 ppm) indicated that part of compound **8** is in the linkage of the [β-Glc*p*-(1 → 4)]-α-Glc*p* II-(1 → 4)-α-Glc*p* I-(1 → 2)-β-Fru*f* I (Fig. S75) (Table 4). Thus, compound **8** was assigned to *O*-β-D-Fru*f*-(2 → 6)-[*O*-β-D-Glc*p*-(1 → 4)]-*O*-α-D-Glc*p*-(1 → 4)-*O*-α-D-Glc*p*-(1 → 2)-*O*-β-D-Fru*f* (Fig. 1).

In addition to the above eight oligosaccharides (**1**–**8**), known sucrose was elucidated for the first time from the aqueous fractions of *S. yildirimlii* and *S. zorkunensis*.

Oligosaccharides based on sucrose have been identified in many plants and have a wide variety of compositions. The most common representatives are saccharides constructed from sucrose and one or more additional glucose molecules. In another group, raffinose and its homologs were found to be related to fructans. However, these occurrences are more restricted. Trehalose is a non-reducing disaccharide, similar to sucrose, and several derived oligosaccharides have been reported in various organisms [26]. The role of trehalose as an anti-stress factor has been reported in several studies, and the biological functions of trehalose and related oligosaccharides are well understood [48]. Trehalose protects proteins, biomembranes, and bacterial cells from freezing temperatures [20,23,37]. All isolated oligosaccharides (**1**–**8**)

are found to be the derivatives of sucrose or trehalose.

A comprehensive review of carbohydrate constituents of the genus *Scorzonera* L. revealed maltose from *S. laciniata*, *S. suberosa*, arabinose from *S. suberosa*, fructose from *S. laciniata*, *S. latifolia*, *S. suberosa*, glucose from *S. laciniata*, *S. latifolia*, *S. suberosa* [49], and sucrose from *S. austriaca* [50], *S. laciniata*, *S. latifolia*, *S. suberosa* [49], *S. hispanica* [51], *S. mongolica* [9], and *S. tomentosa* [52]. Oligosaccharides have been isolated and reported from various natural sources, including *Polygala senega* L. [39], *Gentiana* species [53], and *Asparagus officinalis* L [37].

3.2. Biological activities

Within the scope of this study, the biological activities of the compounds were evaluated through preliminary screening experiments conducted at a single concentration of 100 μM. Compounds **1**–**8** were found to have purities of 88.6–93.6 % (**1**: 91.5 %; **2**: 89.3 %; **3**: 90.2 %, **4**: 88.1 %, **5**: 91.7 %; 6: 92.2 %; 7: 93.6 %, and **8**: 88.6 %) after HPLC analysis. The data obtained provide preliminary information on the potential effects of the compounds on the relevant biological target, and detailed kinetic analyses based on the dose–response relationship have not been performed at this stage. Therefore, IC_{50} values have not been calculated, and the results are reported only at the preliminary screening level. It is believed that the tests were error-free.

3.2.1. Antimicrobial activity

The antimicrobial activities of **1**–**8** were evaluated against six microorganisms (two Gram-negative, two Gram-positive, one mycobacterium, and one yeast fungus) [31,32]. The antimicrobial activities of isolated compounds (**1**–**8**) are listed in Table 5. All tested compounds exhibited anti-pseudomonal and anti-tuberculosis activities. Compounds **2**, **3**, **1**, and **4** exhibited high anti-pseudomonal activity at low concentrations (12.5–55.0 μg/mL), respectively. All compounds except compound **8** exhibited strong anti-tuberculosis activity, but compounds **2**, **3**, **1**, **5**, and **7** exhibited activities at low concentrations of 3.13–15.00 μg/mL, respectively. None of the compounds were effective against Gram-negative enteric bacteria, Gram-positive spore-forming bacilli, and yeast (except compound **5**). Compounds **4**, **7**, and **8** were effective against gram-positive cocci at relatively high concentrations (110–250 μg/mL). Unlike other compounds, compound **5** appeared to be effective against the yeast fungus *C. albicans* at a concentration of 232 μg/mL. These results confirmed the antimicrobial potential of certain oligosaccharide compounds from *S. yildirimlii* and *S. zorkunensis*, providing a promising direction for future antimicrobial treatments.

Table 5
Screening for the antimicrobial activity of oligosaccharides **1**–**8** isolated from *S. yildirimlii* and *S. zorkunensis*.

Microorganisms and minimal inhibitory concentration (MIC, μg/mL)							
Comp.	Stock Sol. (μg/mL)	*Gram (−) Bac.*		*Gram (+) Bac.*		*No Gr.*	*Fungi*
		Ec	Pa	Sa	Bc	Ms	Ca
1	1300	–	32.5	–	–	4.06	–
2	1000	–	12.5	–	–	3.13	–
3	1100	–	13.7	–	–	3.44	–
4	2200	–	55.0	110	–	27.5	–
5	4700	–	230	–	–	14.69	232
6	4600	–	230	–	–	57.0	–
7	300	–	220	230	–	15.0	–
8	10000	–	250	250	–	125	–
Amp.	10	10	>128	35	15	–	–
Strep.	10					4	
Flu.	5						8

Ec: Escherichia coli ATCC35218, *Pa*: *Pseudomonas aeruginosa* ATCC43288, *Sa*: *Staphylococcus aureus*, *Bc*: *Bacillus cereus* 709 Roma, *Ms*: *Mycobacterium smegmatis* ATCC607, *Ca*: *Candida albicans* ATCC60193, Amp.: Ampicillin, Strep.: Streptomycin, Flu.: Fluconazole, (−): no activity.

Table 6
Screening for the enzyme inhibition of oligosaccharides **1**–**8** from *S. yildirimlii* and *S. zorkunensis*.

Compounds	Tyrosinase	α-glucosides
1	19.02 ± 5.89	56.89 ± 1.78
2	14.18 ± 3.30	68.04 ± 4.68
3	nd	24.97 ± 1.65
4	39.78 ± 10.29	28.26 ± 5.22
5	18.16 ± 2.51	25.48 ± 1.63
6	21.31 ± 3.82	9.22 ± 0.93
7	29.59 ± 3.02	nd
8	25.29 ± 2.04	48.83 ± 1.15
Kojic acid	70.01 ± 1.64	–
Acarbose	–	98.89 ± 0.06

nd: Not detected.

M. smegmatis typically causes skin infections. However, lung infection in children with IFN-γ receptor deficiency has also been reported. The most effective treatment for skin, soft tissue, and bone infections caused by *M. smegmatis* typically involves a combination of long-term antibiotic therapy and surgical intervention. *M. smegmatis* is resistant to isoniazid and rifampin, both of which are used to treat infection. However, cefoxitin and cefmetazole have moderate antimicrobial activities. In contrast, known isolates are susceptible or intermediate to non-β-lactam agents, including imipenem, doxycycline, sulfamethoxazole, amikacin, and ciprofloxacin. The chemical structures of the isolated compounds (**1**–**8**) were very similar to those of amikacin and streptomycin, which are used to treat infections caused by *M. smegmatis*. Studies have investigated the antimicrobial activities of extracts or compounds isolated from *Scorzonera* spp. [12,13]. The isolated compounds were oligosaccharides, and, in the structure-activity relationship analysis, trisaccharides were more effective than tetra- and pentasaccharides. Oligosaccharides with fewer monosaccharide units are more effective because of their greater molecular freedom.

3.2.2. Tyrosinase and α-glucosidase enzyme inhibition

The inhibitory effects of compounds **1**–**8** on tyrosinase and α-glucosidase inhibition were investigated and are presented in Table 6, which shows a trend of inhibition at the tested concentrations. Tyrosinase inhibition of **4**, **7**, and **8** exhibited moderate inhibitory activity at 39.78 ± 10.29 %, 29.59 ± 3.02 %, and 25.29 ± 2.04 %, respectively. In addition, compounds **6** (21.31 ± 3.82), **1** (19.02 ± 5.89 %), **5** (18.16 ± 2.51 %), and **2** (14.18 ± 3.30 %) showed mild inhibition, while compound **3** showed no inhibition. All the tested compounds were less effective than the positive control, kojic acid (70.01 ± 1.64 %). α-Glucosidase inhibition of **2** (68.04 ± 4.68 %), **1** (56.89 ± 1.78 %), and **8** (48.83 ± 1.15 %) exhibited the highest activity among the tested compounds **1**–**8**. Compounds **4** (28.26 ± 5.22 %), **5** (25.48 ± 1.63 %), and **3** (24.97 ± 1.65 %) were moderately active. Furthermore, compound **6** (9.22 ± 0.93 %) exhibited weak activity, whereas compound **7** showed no inhibitory effect. All the tested compounds were less effective than acarbose (98.89 ± 0.06 %). This study reveals that compounds **2**, **1**, and **8** are promising candidates for the α-glucosidase inhibitory potential. In a study, Sezer-Senol and colleagues investigated the inhibitory potential of methanol extracts obtained from the aerial parts and roots of 27 *Scorzonera* species at a concentration of 100 mg/mL on acetylcholine/butyrylcholinesterase (AChE/BuChE), and tyrosinase enzymes. They found that the extracts weakly inhibited AChE (3.75 ± 0.71–15.97 ± 0.43 %) and BuChE (2.08 ± 1.35 %–25.32 ± 1.37 %). The highest effect on tyrosinase was found in *S. pisidica* aerial parts (40.25 ± 0.74 %) and chlorogenic acid (46.97 ± 0.82 %) [1]. Studies on enzyme inhibition have been performed using extracts and isolated compounds of *Scorzonera* species [12,13]. Considering the results, it can be concluded that the Scorzonera species possess inhibitory potential against tyrosinase and α-glucosidase, as evidenced by this study.

3.2.3. Cell viability assay

The cytotoxic activity of compounds **1**–**8** against L-929 cells has been investigated [35]. The results showed that compounds **1** and **2** exhibited no or weak growth inhibition at the tested concentrations (0.3–100 μg/mL). Compounds **1**–**8** exhibit nearly identical cytotoxic activities against L-929 cells. Cell viability (%) values ranged from 81 ± 4.9 to 88 ± 2.05 % at concentrations up to 100 μg/mL, following 24 h exposure (Fig. 2). Numerous cytotoxicity evaluations of isolates of *Scorzonera species* have been reported in the literature [12,13]. The cytotoxic activities of platyphylloside, scorzoneric acid, and scorzonerin, isolated from *S. divaricata* and *S. pseudodivaricata* were investigated against the

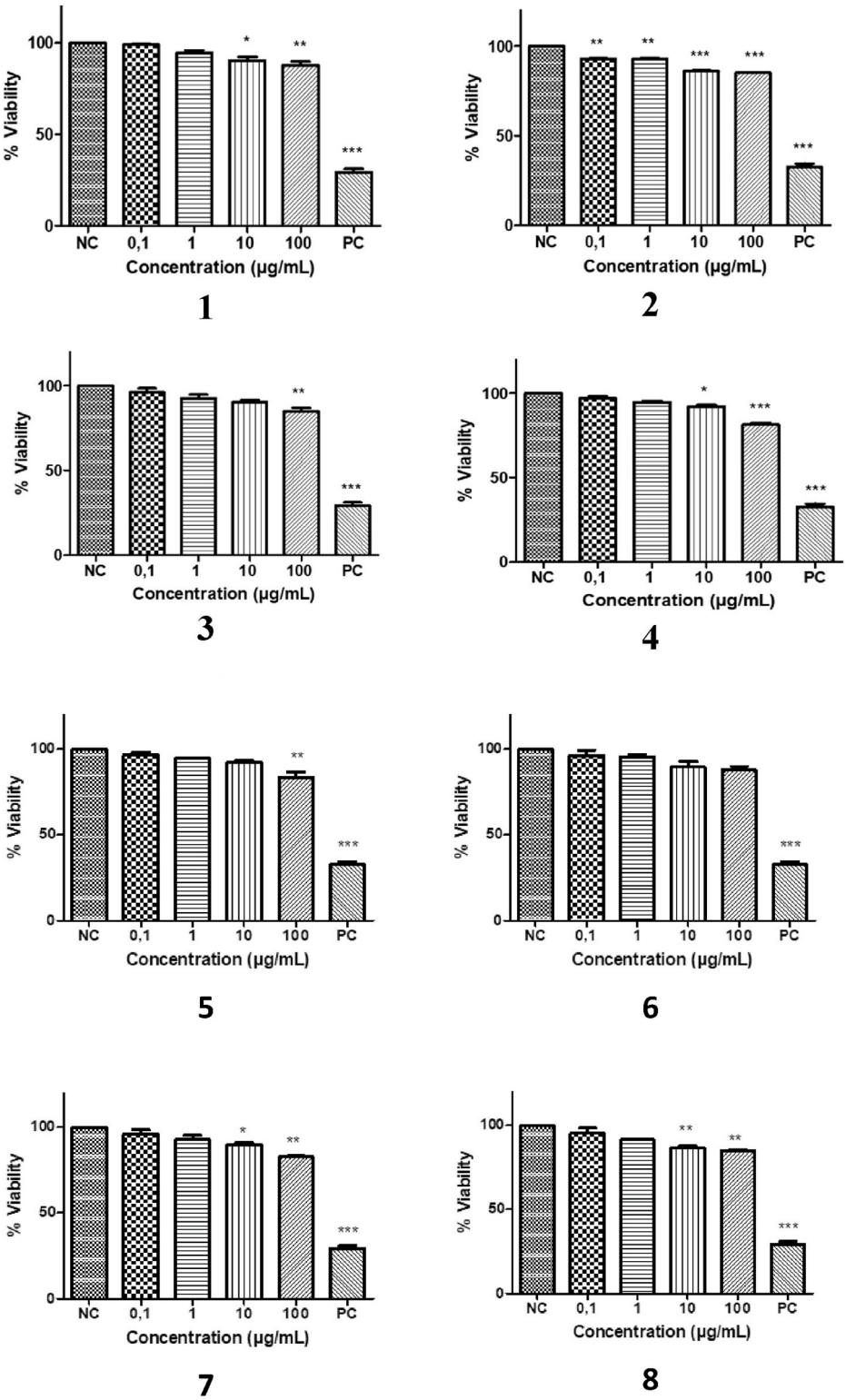


Fig. 2. MTT assay results of compounds **1**–**8** in L-929 cells. NC: Negative control. PC: Positive control. *: $p < 0,05$; **: $p < 0,01$; ***: $p < 0,001$. One-way ANOVA test was used to assess whether there was a statistically significant difference between the control group and the extracts. The Tukey test was used as a post test. All tests were performed using the Graphpad Prism 5.1 program.

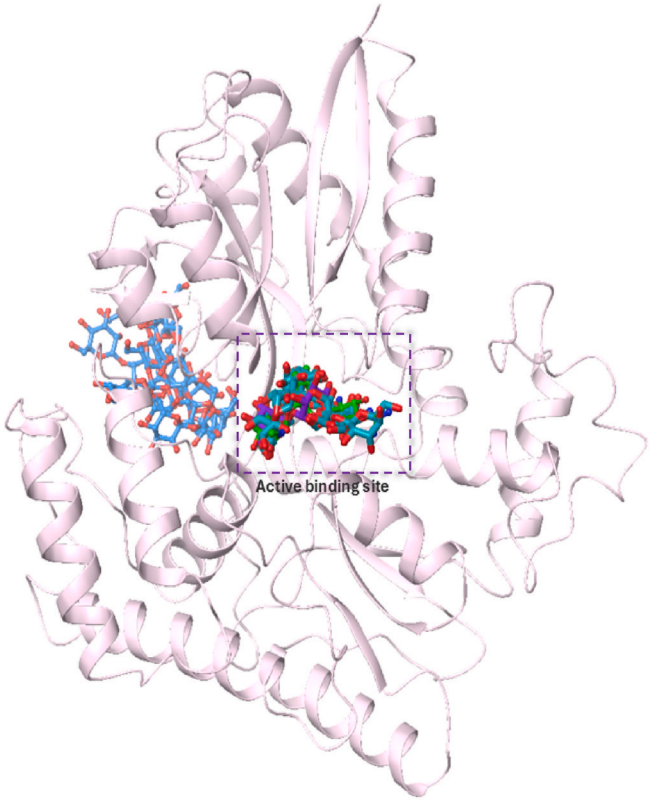


Fig. 3. Binding modes of compounds **1**–**8** in the crystal structure of the Trehalose-LpqY complex. Purple: protein; Green: streptomycin; Cyan: compounds **1**–**4**; Blue: compounds **5**–**8**. (For interpretation of the references to colour in this figure legend, the reader is referred to the Web version of this article.)

mouse lymphoma cell line (L5175Y) and exhibited over 90 % cell growth inhibition [5]. The cytotoxicity of the pure substances isolated from *S. mongolica* was evaluated against the A549 cell line [9]. Sulfoscorzonine A-C and scorcodivaricin A-C isolated from *S. divaricata* were tested against HL-60, HeLa, HepG2, and SMMC-7721 cells, and Scorcodivaricin B exhibited significant cytotoxic activity with IC_{50} values of 24.4 μM, 24.5 μM, 36.2 μM, and 66.7 μM, respectively [54]. The pure compounds isolated from the roots of *S. judaica* were cytotoxic against MCF7 (Human breast adenocarcinoma) [55]. There was no cytotoxic activity of *S. austriaca* isolates against the BEL-7404 and HL-60 cell lines [56]. Cytotoxicity is the primary step in classifying compounds as therapeutic agents. The isolated compounds were oligosaccharides, and cytotoxic effects were not observed as expected. Thus, it is evident that the O- and C-glycosidic compounds are biologically effective.

3.3. Molecular docking study

Molecular docking was performed to predict the binding modes of the compounds at the enzyme's active site. In molecular docking studies, the crystal structure of the Trehalose-LpqY complex (Protein Data Bank (PDB): 7APE) [25], isolated from the *Mycobacterium thermoresistible* strain, was identified as the most effective in biological activity assays. These compounds were found to bind to the same region as the known inhibitor compound in the Trehalose-LpqY complex structure (Fig. 2). Similar to these compounds, compound **4** binds to the same region but with a conformation different from that of the other compounds. Consequently, it may not interact with certain sites, resulting in lower enzyme inhibition (MIC = 27.5 μg/mL) than with the other derivatives. Molecular docking studies revealed that compounds **5**–**8** (MIC = 14.69–125 μg/mL), which were ineffective against the *M. thermoresistable* strain in the biological activity studies, were docked in a different region than the known inhibitor compound in the trehalose-LpqY complex structure. This resulted in the loss of important interactions. These derivatives are thought to be unable to bind to the active site due to their additional cyclic structures (Fig. 3).

According to molecular docking results, compounds **1**–**4** bind to the same region as Streptomycin, which is used as a positive control in biological activity studies and is also a known inhibitor of the Trehalose-LpqY complex. Owing to differences in group and volumetric properties, the compounds bind to distinct amino acids within the active binding region and form more hydrogen-bond interactions. **1**, **2**, and **3**, which showed high inhibitory activity against the *M. thermoresistable* strain in biological assays, formed numerous hydrogen-bond interactions with the amino acids Glu118, Glu190, and Asp199. Among these compounds, **2** had a binding energy of −11.088 kcal/mol and showed higher biological activity than other derivatives. These interactions are important for inhibitory activity. **4** was found to bind to the same region as these compounds (**1**, **2**, and **3**) but lacked the Asp199 bond. This loss of interaction was thought to be the reason for the low inhibitory activity of **4** (Table 7, Fig. 4). According to the findings of the molecular docking study, compound **8** was found to have a high number of interactions and the best binding score in the Trehalose-LpqY complex due to the free hydroxyl groups in its structure. When compared to compounds **1**, **2**, and **3**, which were determined to have the strongest inhibitory activity against the *M. thermoresistible* strain in biological activity studies, compound **8** was found to have lower activity. It was determined that compound **8** binds to a different region than these compounds due to its structural properties. It is thought that the different binding site of compound **8** causes a loss of biological activity.

4. Conclusion

The chemical studies of *S. yildirimlii* and *S. zorkunensis* led to the identification of eight new oligosaccharides (**1**–**8**), which were reported for the first time. Compounds **1**–**4** showed promising antimicrobial activity against *M. bacterium* without exhibiting significant toxicity. In the MD study of compounds **1**, **2**, and **3**, which exhibited high inhibitory activity against the *M. bacterium* strain at the tested concentrations, it was determined that they formed numerous hydrogen bond interactions with the amino acids Glu118, Glu190, and Asp199. Compound **8** exhibited the highest number of interactions and the best binding score in the Trehalose–LpqY complex, likely due to the presence of free hydroxyl groups in its structure. Despite these favorable docking results, compound **8** exhibited lower inhibitory activity against the *M. thermoresistible* strain than compounds **1**, **2**, and **3**, which

Table 7
Binding energy values and interactions for the crystal structure of the Trehalose-LpqY complex in the active site of compounds **1**–**8.**

ID	XP Glide score (kcal/mol)	Interactions with amino acids
1	−11.769	Glu118, Asn123, Gly124, Glu190, Leu197, Ser198, Asp199, Arg404
2	−11.088	Glu118, Lys121, Asn123, Glu190, Ser198, Asp199, Arg329
3	−11.860	Glu118, Glu190, Ser198, Asp199
4	−11.643	Glu118, Glu190, Arg329, Leu398, Ile399
5	−11.744	Glu190, Arg329, Leu398, Ile399, Ala406
6	−14.297	Glu118, Asp199, Arg329, Ile399
7	−12.310	Glu118, Glu190, Leu197, Ser198, Asp199, Arg329, Ala401
8	−15.320	Glu118, Glu190, Leu197, Leu398, Ile399, Val403
Strep.[a]	−6.638	Asn25, Gln59, Asn134, Glu241, Asn242, Gly334
Coligand	−12.585	Asn25, Glu26, Gln59, Asp80, Asn134, Glu241, Gly334, Arg404

[a] Strep.: Streptomycin.

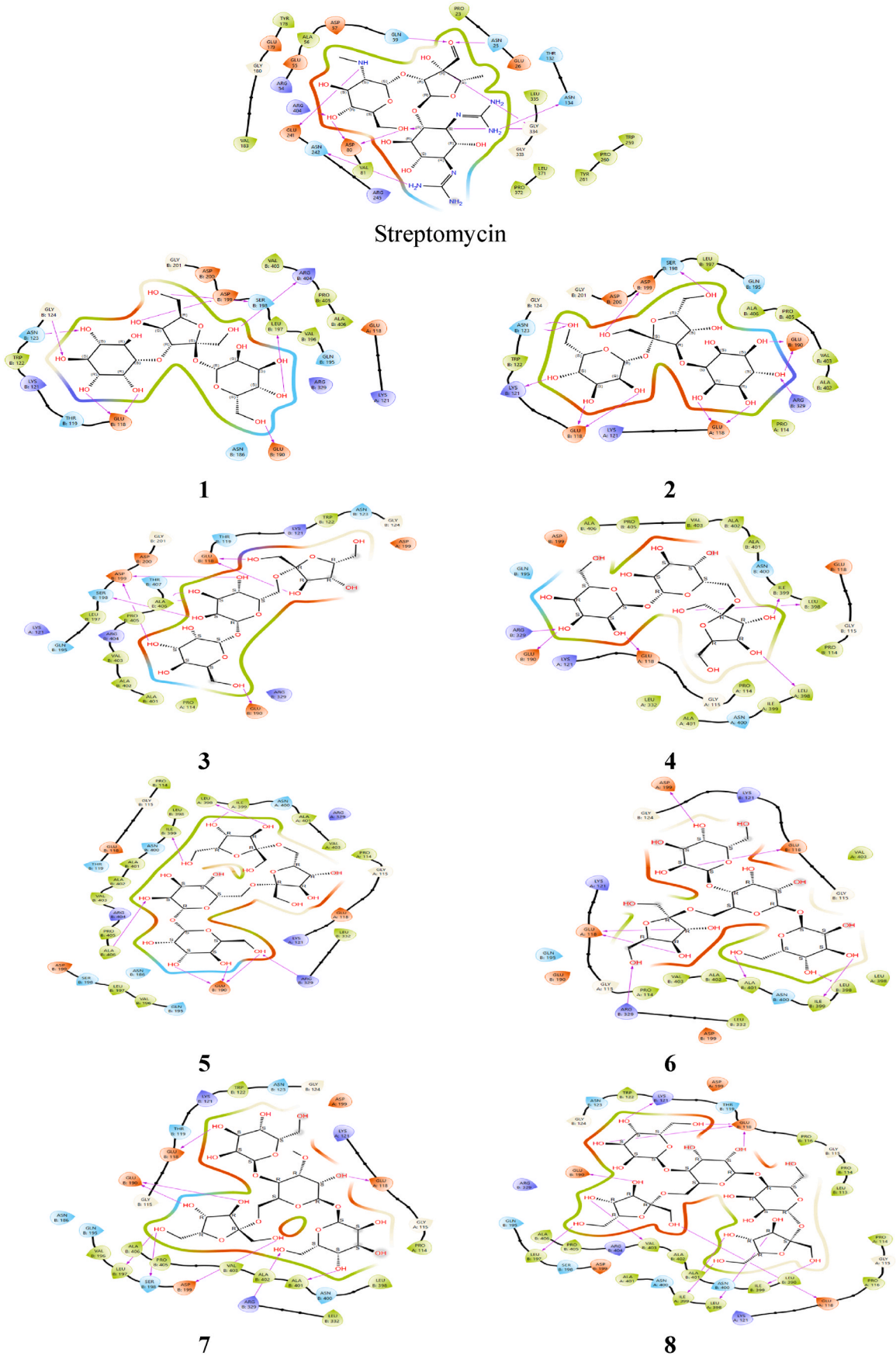


Fig. 4. 2D Structures of binding poses of **1**–**8** in the crystal structure (PDB: 7APE) of the Trehalose-LpqY complex. Purple: hydrogen bonds. (For interpretation of the references to colour in this figure legend, the reader is referred to the Web version of this article.)

demonstrated the strongest biological activity. Among them, **2** had a binding energy of −11.088 kcal/mol and exhibited higher biological activity than the other derivatives.

Structural analysis indicated that compound **8** binds to an allosteric or non-critical region of the target protein, and this alternative binding site is considered a key factor contributing to its reduced biological activity. Docking scores are computational measures that quantify the thermodynamic binding affinity between a ligand and a target protein, primarily reflecting static binding affinity. These scores represent the theoretical sum of interactions, such as hydrogen bonds, hydrophobic interactions, and electrostatic contributions, that the ligand forms within the binding site. However, because docking approaches largely assume the protein-ligand system to be rigid, they cannot fully account for dynamic processes critical to biological function, such as conformational changes, solvent effects, binding kinetics, and allosteric regulation. Therefore, high docking scores do not always correlate directly with strong functional inhibition or biological activity; further experimental data could support these results.

MD results for the *M. thermoresistable* strain indicate that compounds **1**–**4** could serve as inhibitors of *M. smegmatis*. Further research is needed to identify specific agents that can overcome inhibitor effects on *M. bacterium*. The isolated compounds (**1**–**8**) are highly similar to the structures of streptomycin and amikacin, which are antibiotics used to treat various bacterial infections, including tuberculosis. This suggests potential use against *M. smegmatis* infections. Isolated compounds **1**–**8** showed almost no cytotoxic activity in L-929 cells. Based on these results, further *in vivo* studies may be planned for the isolated oligosaccharide compounds for pharmacological use.

CRediT authorship contribution statement

Nurettin Yaylı: Writing – review & editing, Writing – original draft, Project administration, Conceptualization. **Büşra Korkmaz:** Writing – review & editing. **Gozde Bozdal:** Writing – review & editing, Writing – original draft, Visualization, Project administration. **Büşra Şahin:** Writing – review & editing. **Şeyma Arıcı:** Writing – original draft. **Yasemin Altun Ali:** Writing – original draft. **Sermet Yıldırmış:** Writing – original draft. **Gökçe Seyhan:** Writing – original draft. **Ahmet Buğra Aksel:** Writing – original draft. **Kamil Coşkunçelebi:** Writing – original draft. **Serdar Makbul:** Writing – original draft. **Arif Bozdeveci:** Writing – original draft.

Declaration of competing interest

The authors declare the following financial interests/personal relationships which may be considered as potential competing interests: Prof. Dr. Nurettin yayli reports a relationship with Karadeniz Technical University that includes: consulting or advisory. If there are other authors, they declare that they have no known competing financial interests or personal relationships that could have appeared to influence the work reported in this paper.

Acknowledgments

This work was supported by the Scientific and Technological Research Council of Turkiye (TÜBİTAK, Project No. 123Z508). We also thank Karadeniz Technical University for the financial support (Project No. KTÜ-BAP 8133).

Appendix A. Supplementary data

Supplementary data to this article can be found online at https://doi.org/10.1016/j.carres.2026.109833.

Data availability

sup.metarial

References

[1] F. Sezer Senol, S. Bahadır Açıkara, G. Saltan Çıtoğlu, I. Erdoğan-Orhan, S. Dall'Acqua, F. Özgökçe, Prospective neurobiological effects of the aerial and root extracts and some pure compounds of randomly selected *Scorzonera* species, Pharm. Biol. 52 (2014) 873–882, https://doi.org/10.3109/13880209.2013.872152.

[2] D. Chamberlain, L. Scorzonera, in: P.H. Davis (Ed.), Flora of Turkey and the East Aegean Islands, vol. 5, Edinburgh Univ. Press, Edinburgh, 1975, pp. 632–657.

[3] G.S. Çitoğlu, Ö. Bahadır, S. Dall'Acqua, Dihydroisocoumarin derivatives isolated from the roots of *Scorzonera latifolia*, Turk. J. Pharm. Sci. 7 (2010) 205–212.

[4] S. Makbul, Z. Türkmen, K. Coşkunçelebi, O. Beyazoğlu, Morphometric study on *scorzonera* L. taxa (Asteraceae) from northeast Anatolia, Acta Bot. Croat. 69 (2010) 237–247.

[5] N. Tsevegsuren, R. Edrada, W. Lin, R. Ebel, C. Torre, S. Ortlepp, V. Wray, P. Proksch, Biologically active natural products from Mongolian medicinal plants *Scorzonera divaricata* and *Scorzonera pseudodivaricata*, J. Nat. Prod. 70 (2007) 962–967, https://doi.org/10.1021/np070013r.

[6] B. Wang, G.Q. Li, H.S. Guan, L.Y. Yang, G.Z. Tong, A new erythrodiol triterpene fatty ester from *Scorzonera mongolica*, Acta Pharm. Sin. 44 (2009) 1258–1261.

[7] T. Baytop, Therapy with Medicinal Plants in Turkey, Nobel Publishers, Istanbul, 1999.

[8] E. Sezik, E. Yeşilada, M. Tabata, G. Honda, Y. Takaishi, T. Fujita, T. Tanaka, Y. Takeda, Traditional medicine in Turkey VIII, Folk Med. East Anatolia; Erzurum, Erzincan, Ağrı, Kars, Iğdır provinces, Econ Bot. 51 (1997) 195–211, https://doi.org/10.1007/BF02862090.

[9] B. Wang, P.J. Qiu, G.Q. Li, Y.L. Qu, Antitumor constituents from *Scorzonera mongolica*, Chin. J. Nat. Med. 7 (2009) 283–286, https://doi.org/10.3724/sp.j.1009.2009.00283.

[10] Y. Zhu, Q.X. Wu, P.Z. Hu, W.S. Wu, Biguaiascorzolides A and B: two novel dimeric guaianolides with a rare skeleton, from *Scorzonera austriaca*, Food Chem. 114 (2009) 1316–1320, https://doi.org/10.1016/j.foodchem.2008.11.009.

[11] C. Zidorn, E.P. Ellmerer-Müller, H. Stuppner, Tyrolobibenzyls-novel secondary metabolites from *Scorzonera humilis*, Helv. Chim. Acta 83 (2000) 2920–2925, https://doi.org/10.1002/1522-2675(20001108)83:11%3C2920::aid-hlca2920%3E3.0.co;2-5.

[12] Y. Gong, Z.N. Shi, J. Yu, X.F. He, X.H. Meng, Q.X. Wu, Y. Zhu, The genus *Scorzonera* L. (Asteraceae): a comprehensive review on traditional uses, phytochemistry, pharmacology, toxicology, chemotaxonomy, and other applications, J. Ethnopharmacol. 320 (2024) 116787, https://doi.org/10.1016/j.jep.2023.116787.

[13] K. Lendzion, A. Gornowicz, K. Bielawski, A. Bielawska, Phytochemical composition and biological activities of *Scorzonera* species, Int. J. Mol. Sci. 22 (2021) 5128, https://doi.org/10.3390/ijms22105128 (2021).

[14] B. Korkmaz, G. Renda, G. Bozdal, K. Coşkunçelebi, A. Bozdeveci, U. Uzuner, N. Yaylı, Dihydroisocoumarins and phenylglycosides from *Scorzonera longiana*, their antimicrobial activities and molecular docking studies, Chem. Biodivers. 20 (20) (2023) e202201052, https://doi.org/10.1002/cbdv.202201052.

[15] B. Korkmaz, G. Renda, İ. Erik, G. Kılıç, K. Coşkunçelebi, N. Yaylı, Two new dihydroisocoumarins and terpenoids from *Scorzonera longiana* Sümbül, an endemic species to Turkey, and their antimicrobial activity, Nat. Prod. Res. 37 (2023) 1185–1198, https://doi.org/10.1080/14786419.2021.2000410.

[16] I. Erik, N. Yaylı, K. Coşkunçelebi, S. Makbul, S.A. Karaoğlu, Three new dihydroisocoumarin glycosides with antimicrobial activities from *Scorzonera aucheriana*, Phytochem. Lett. 43 (2021) 45–52, https://doi.org/10.1016/j.phytol.2021.02.010.

[17] T. Abe, H. Kikuchi, T. Aritsuka, Y. Takata, E. Fukushi, Y. Fukushi, N. Shiomi, Structural confirmation of novel oligosaccharides isolated from sugar beet molasses, Food Chem. 202 (2016) 284–290, https://doi.org/10.1016/j.foodchem.2016.01.126.

[18] A. Elbermawi, F. Zulfiqar, S.I. Khan, I.A. Khan, Z. Ali, Phytochemical analysis of *Cichorium bottae* root and anti-inflammatory potential assessment of isolates, Fitoterapia 177 (2024) 106106, https://doi.org/10.2139/ssrn.4821375.

[19] H.M. Hammoda, N.M. Ghazy, F.M. Harraz, M.M. Radwan, M.A. ElSohly, I. I. Abdallah, Chemical constituents from *Tribulus terrestris* and screening of their antioxidant activity, Phytochemistry 92 (2013) 153–159, https://doi.org/10.1016/j.phytochem.2013.04.005.

[20] M. Muramatsu, T. Nakakuki, Enzymatic synthesis of novel fructosyl and oligofructosyl trehaloses by *Aspergillus sydowi* β-fructofuranosidase, Biosci. Biotechnol. Biochem. 59 (1995) 208–212, https://doi.org/10.1271/bbb.59.208.

[21] J. Seibel, R. Moraru, S. Götze, K. Buchholz, S. Na'amnieh, A. Pawlowski, H. J. Hecht, Synthesis of sucrose analogues and the mechanism of action of *Bacillus subtilis* fructosyltransferase (levansucrase), Carbohydr. Res. 341 (2006) 2335–2349, https://doi.org/10.1016/j.carres.2006.07.001.

[22] E. Vinogradov, K. Bock, Structural determination of some new oligosaccharides and analysis of the branching pattern of isomalto oligosaccharides from beer, Carbohydr. Res. 309 (1998) 57–64, https://doi.org/10.1016/s0008-6215(98)00119-0.

[23] C.T. Fransen, K.M. Van Laere, A.A. Van Wijk, L.P. Brüll, M. Dignum, J.E. Thomas-Oates, J.F. Vliegenthart, α-D-Glcp-(1→1')-β-D-Galp-containing oligosaccharides,

novel products from lactose by the action of β-galactosidase, Carbohydr. Res. 314 (1998) 101–114, https://doi.org/10.1016/s0008-6215(98)00285-7.
[24] S.J. Angyal, L. Odier, The ^{13}C-NMR spectra of inositols and cyclohexanepentols: the validity of rules correlating chemical shifts with configuration, Carbohydr. Res. 100 (1982) 43–54, https://doi.org/10.1016/s0008-6215(00)81024-1.
[25] C.M. Furze, I. Delso, E. Casal, C.S. Guy, C. Seddon, C.M. Brown, H.L. Parker, A. Radhakrishnan, R. Pacheco-Gomez, R.J. Stansfeld, J. Angulo, A.D. Cameron, E. Fullam, Structural basis of trehalose recognition by the mycobacterial LpqY-SugABC transporter, J. Biol. Chem. 296 (2021) 100307, https://doi.org/10.1016/j.jbc.2021.100307.
[26] M. Nishizawa, S. Kodama, Y. Yamane, K. Kayano, S. Hatakeyama, H. Yamada, Synthesis and glycosylation shift of 1,1′-disaccharides, Chem. Pharm. Bull. 42 (1994) 982–984, https://doi.org/10.1002/chin.199449238.
[27] H. Okada, E. Fukushi, S. Onodera, T. Nishimoto, J. Kawabata, M. Kikuchi, N. Shiomi, Synthesis and structural analysis of five novel oligosaccharides prepared by glucosyltransfer from *β*-D-glucose 1-phosphate to isokestose and nystose using *Thermoanaerobacter brockii* kojibiose phosphorylase, Carbohydr. Res. 338 (2003) 879–885, https://doi.org/10.1016/s0008-6215(03)00020-x.
[28] J. Song, Y. Liu, X. Yin, Y. Nan, Y. Shi, X. Chen, H. Liang, J. Zhang, B. Ma, Isolation and structural elucidation of prebiotic oligosaccharides from Ziziphi Spinosae Semen, Carbohydr. Res. 534 (2023) 108948, https://doi.org/10.1016/j.carres.2023.108948.
[29] S. Paraschos, P. Magiatis, E. Kalpoutzakis, C. Harvala, A.L. Skaltsounis, Three new dihydroisocoumarins from the Greek endemic species *Scorzonera cretica*, J. Nat. Prod 64 (2001) 1585–1587, https://doi.org/10.1021/np0103665.
[30] K. Çoşkunçelebi, S. Makbul, M. Gültepe, S. Okur, M.E. Güzel, A conspectus of *Scorzonera* s.l. in Turkey, Turk. J. Bot. 39 (2015) 76–87, https://doi.org/10.3906/bot-1401-10.
[31] G. Bozdal Korkmaz, E. Koç, B. Şahin, E. Öztürk, S. Fandaklı, Ş. Alpay Karaoğlu, N. Yaylı, Essential oils, phenolic contents, and antimicrobial activities of *Vicia bithynica* L. and *Vicia cracca* L. subsp. *cracca*, Chem. Biodivers. (2025) e00813, https://doi.org/10.1002/cbdv.202500813 (2025), 0.
[32] A.L. Barry, Methods for determining bactericidal activity of antimicrobial agents: approved guideline, Natl. Comm. Clin. Lab. Stand. 19 (1999) 18.
[33] G.L. Woods, B.A. Brown-Elliott, E.P. Desmond, G.S. Hall, L. Heifets, G.E. Pfyffer, J. C. Ridderhof, R.J. Wallace, N.C. Warren, F.G. Witebsky, Susceptibility Testing of Mycobacteria, Nocardiae, and Other Aerobic Actinomycetes, 2003, https://doi.org/10.1128/9781555816728.ch73. Approved standard, NCCLS Document M24-A.
[34] N. Yaylı, G. Kılıç, N. Kahriman, Ş. Kanbolat, A. Bozdeveci, Ş.A. Karaoğlu, R. Aliyazıcıoğlu, H.E. Sellitepe, İ.S. Doğan, A. Aydın, G. Tatar, Synthesis, biological evaluation (antioxidant, antimicrobial, enzyme inhibition, and cytotoxic) and molecular docking study of hydroxy methoxy benzoin/benzil analogous, Bioorg. Chem. 115 (2021) 105183, https://doi.org/10.1016/j.bioorg.2021.105183.
[35] C.Ö. Yalçın, S.Y. Sarıaltın, D.Ç. Polat, Quantification of phenolic and flavonoid contents and some biological activities of Ornithogalum sigmoideum Freyn & Sint, J. Pharm. Res. 24 (2020) 487–496, https://doi.org/10.35333/jrp.2020.197.
[36] R.A. Friesner, R.B. Murphy, M.P. Repasky, L.L. Frye, J.R. Greenwood, T.A. Halgren, P.C. Sanschagrin, D.T. Mainz, Extra precision glide: docking and scoring incorporating a model of hydrophobic enclosure for protein–ligand complexes, J. Med. Chem. 49 (2006) 6177–6196, https://doi.org/10.1021/jm051256o.s001.
[37] E. Fukushi, S. Onodera, A. Yamamori, N. Shiomi, J. Kawabata, NMR analysis of tri- and tetrasaccharides from asparagus, Magn. Reson. Chem. 38 (2000) 1005–1011, https://doi.org/10.1002/1097-458X(200012)38:12<1005::AID-MRC772>3.0.CO;2-Q.
[38] N. Kawazoe, H. Okada, E. Fukushi, A. Yamamori, S. Onodera, J. Kawabata, N. Shiomi, Structural analysis of two trisaccharides isolated from fermented beverage of plant extract, Open Glycosci. 1 (2008) 25–30, https://doi.org/10.2174/1875398100801010025.
[39] H. Saitoh, T. Miyase, A. Ueno, Senegoses A-E, oligosaccharide multi-esters from *Polygala senega* var. *latifolia* Torr. *et* Gray, Chem. Pharm. Bull. 41 (1993) 1127–1131, https://doi.org/10.1248/cpb.41.1127.
[40] M. Vanhaecke, N. Dyubankova, E. Lescrinier, W. Van den Ende, Metabolism of galactosyl-oligosaccharides in *Stellaria media*–Discovery of stellariose synthase, a novel type of galactosyltransferase, Phytochemistry 71 (2010) 1095–1103, https://doi.org/10.1016/j.phytochem.2010.04.012.
[41] K.J. Steadman, D.J. Fuller, R.L. Obendorf, Purification and molecular structure of two digalactosyl D-*chiro*-inositols and two trigalactosyl D-*chiro*-inositols from buckwheat seeds, Carbohydr. Res. 331 (1) (2001) 19–25, https://doi.org/10.1016/S0008-6215(00)00320-7.
[42] M.P. Thomas, S.J. Mills, B.V. Potter, The “other” inositols and their phosphates: synthesis, biology, and medicine (with recent advances in myo-inositol chemistry), Angew. Chem. Int. Ed. Engl. 55 (5) (2016) 1614–1650, https://doi.org/10.1002/anie.201502227.
[43] S.J. Angyal, L. Odier, The ^{13}C-NMR spectra of inositols and cyclohexanepentols: the validity of rules correlating chemical shifts with configuration, Carbohydr. Res. 100 (1) (1982) 43–54, https://doi.org/10.1016/S0008-6215(00)81024-1.
[44] Y. Sogame, M. Ogata, S. Hakozaki, Y. Saito, T. Suzuki, R. Saito, K. Watanabe, *α,β*-Trehalose, an intracellular substance in resting cyst of colpodid ciliates as a key to environmental tolerances, Biochem. Biophys. Res. Commun. 716 (2024) 149971, https://doi.org/10.1016/j.bbrc.2024.149971.
[45] A. Miranda-Molina, E. Castillo, A.L. Munguia, A novel two-step enzymatic synthesis of blastose, a *β*-D-fructofuranosyl-(2→6)-D-glucopyranose sucrose analogue, Food Chem. 227 (2017) 202–210, https://doi.org/10.1016/j.foodchem.2017.01.094.
[46] I. Pérez-Victoria, J.C. Morales, Regioselectivity in acylation of oligosaccharides catalyzed by the metalloprotease thermolysin, Tetrahedron 62 (2006) 2361–2369, https://doi.org/10.1016/j.tet.2005.11.066.
[47] M. Tanaka, Y. Nakajima, K. Nishio, H. Hashimoto, Structure of oligosaccharides prepared by acidic condensation of palatinose, J. Carbohydr. Chem. 12 (1993) 49–61, https://doi.org/10.1080/07328309308018540.
[48] M. Ohta, Y.T. Pan, R.A. Laine, A.D. Elbein, Trehalose-based oligosaccharides isolated from the cytoplasm of *Mycobacterium smegmatis*: relation to trehalose-based oligosaccharides attached to lipid, Eur. J. Biochem. 269 (2002) 3142–3149, https://doi.org/10.1046/j.1432-1033.2002.02971.x.
[49] Y. Erden, S. Kırbag, Ö. Yılmaz, Phytochemical composition and antioxidant activity of some *Scorzonera* species, Proc. Natl. Acad. Sci. India B Biol. Sci. 83 (2013) 271–276, https://doi.org/10.1007/s40011-012-0129-7.
[50] Z.W. He, Study on the Chemical Constituents of *Cirsium souliei* and *Scorzonera austriaca*, Lanzhou Univ., 2007, pp. 16–29. M.Sc. Thesis.
[51] G. Ak, S. Dall'Acqua, S. Sut, I. Ferrarese, E. Yıldıztugay, M.F. Mahomoodally, K. I. Sinan, N.B. Sadeer, K.R.R. Rengasamy, G. Zengin, Chemical characterization and bio-pharmaceutical abilities of five different solvent extracts from aerial parts and roots of *Scorzonera hispanica* L, S. Afr. J. Bot. 133 (2020) 212–221, https://doi.org/10.1016/j.sajb.2020.08.003.
[52] S. Dall'Acqua, G. Ak, S. Sut, G. Zengin, E. Yıldıztugay, M.F. Mahomoodally, K. I. Sinan, D. Lobine, Comprehensive bioactivity and chemical characterization of the endemic plant *Scorzonera hieraciifolia* Hayek extracts: a promising source of bioactive compounds, Food Res. Int. 137 (2020) 109371, https://doi.org/10.1016/j.foodres.2020.109371.
[53] D.N. Olennikov, N.I. Kashchenko, A.I. Gadimli, D.I. Isaev, Polysaccharides from three species of *Gentiana*, Chem. Nat. Compd. 58 (2022) 799–803, https://doi.org/10.1007/s10600-022-03801-y.
[54] Y.J. Yang, J. Yao, X.J. Jin, Z.N. Shi, T.F. Shen, J.G. Fang, X.J. Yao, Y. Zhu, Sesquiterpenoids and tirucallane triterpenoids from the roots of *Scorzonera divaricate*, Phytochemistry 124 (2016) 86–98, https://doi.org/10.1016/j.phytochem.2016.01.015.
[55] A. Bader, N. de Tommasi, R. Cotugno, A. Braca, Phenolic compounds from the roots of Jordanian viper's grass, *Scorzonera judaica*, J. Nat. Prod. 74 (2011) 1421–1426, https://doi.org/10.1021/np200143s.
[56] Q.X. Wu, Y.B. Su, Y. Zhu, J. Li, W.S. Wu, Triterpenes and steroids from the roots of *Scorzonera austriaca*, Fitoterapia 82 (2011) 493–496, https://doi.org/10.1016/j.fitote.2011.01.006.